JOURNAL OF APPLIED PHYSICS

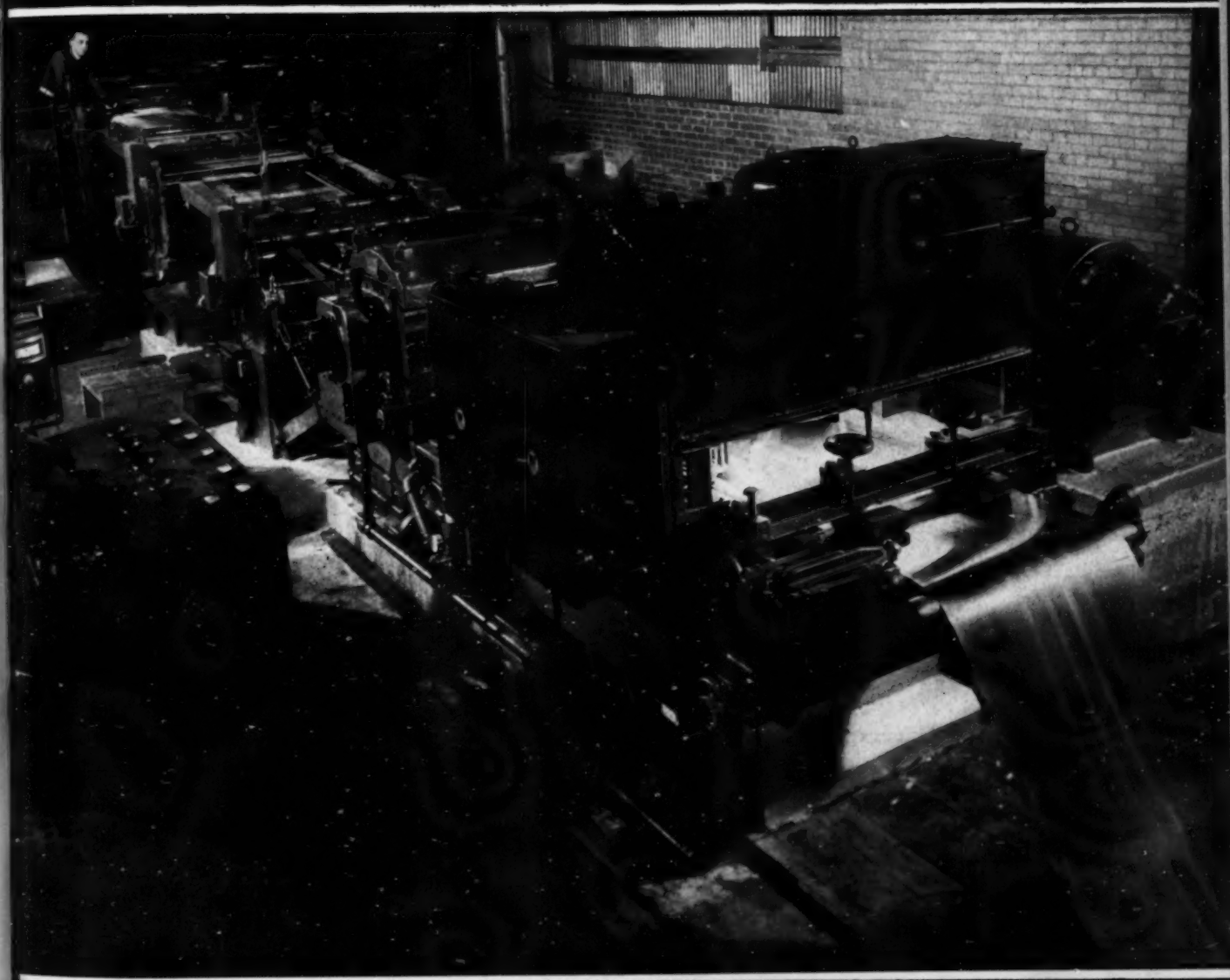

JOURNAL
OF
APPLIED PHYSICS

Vol. 15, No. 5 MAY, 1944

In This Issue

		Page
Organization of Physics in America	W. Waterfall and E. Hutchisson	407
General Vibration of a Hinged Beam	Herbert Kapfel Brown	410
Effect of Thixotropy on Plasticity Measurements	Henry Green and Ruth N. Weltmann	414
Development of the General Antenna Array Equation	William T. Thomson	420
Electron Microscopic Determination of Surface Elevations and Orientations	R. D. Heidenreich and L. A. Matheson	423
Rate of Rise of Water in Capillary Tubes	William A. Rense	436
Mechanical Models of Frequency Converters	Harry Stockman	438
Formation of Bubbles	Robert B. Dean	446
Thermal and Electrical Conductivity of Graphite and Carbon at Low Temperatures	Robert A. Buerschaper	452
Letter to the Editor: Microradiographs and X-Ray Micrographs	Elsie L. Garvin	455

In Every Issue

Calendar of Meetings	455
Here and There	456
New Booklets	456
Recent Applications of Physics	457
Index to Advertisers	xx

BOARD OF EDITORS

Elmer Hutchisson,
Editor

Associate Editors

R. B. Barnes
Otto Beeck
W. F. Busse
S. H. Caldwell
Clark Goodman
Selig Hecht
W. J. Lyons
Morris Muskat
Thomas H. Osgood
Paul E Sabine
Frederick Seitz
J. R Townsend

Publication of the American Institute of Physics

ADMINISTRATIVE STAFF

Henry A. Barton,
Director

Madeline M. Mitchell,
Publications Manager

John T. Tate,
Adviser on Publications

GOVERNING BOARD

Paul E. Klopsteg,
Chairman

George B. Pegram,
Secretary

T. D. Cope
R. B. Dow
L. A. DuBridge
Floyd A. Firestone
Harvey Fletcher
R. C. Gibbs
K. S. Gibson
Arthur C. Hardy
Hermann Mark
A. G. Worthing
John T. Tate
N. W. Taylor
Wallace Waterfall

The Journal of Applied Physics, published monthly at Prince and Lemon Sts., Lancaster, Pa., is devoted to physics in its role as the science basic to other natural sciences and to the arts and industries. Previous to 1937 this publication was known as Physics. The Journal of Applied Physics publishes editorials, news of physicists, and reviews, as well as technical papers of applied physics.

Manuscripts should be submitted to Elmer Hutchisson, Editor, 50th floor, 350 Fifth Avenue, New York 1, New York.

Subscriptions and orders for back numbers should be addressed to Prince and Lemon Streets, Lancaster, Pa. or to the American Institute of Physics, 57 East 55 Street, New York 22, N. Y.

Subscription Price

	U. S. and Canada	Elsewhere
To members of scientific societies	$5.00	$5.70
To all others	7.00	7.70

Back Number Prices

Complete set: Vol. 1, July, 1931–Vol. 14, 1943—**$87.50**
Yearly back number rate: **$7.70**
Single copies: **$0.70** each.

Changes of address and proofs should be addressed to the Publications Manager.

Advertising rates supplied on request. Orders, advertising copy, and cuts should be sent to the American Institute of Physics.

Entered as second class matter January 22, 1937, at the Post Office at Lancaster, Pennsylvania, under the Act of March 3, 1879.
Accepted for mailing at the special rate of postage provided for in the Act of February 28, 1925, authorized May 2, 1932.

Copyright 1944, by the American Institute of Physics.

Journal
of
Applied Physics

Volume 15, Number 5 May, 1944

Organization of Physics in America

IN a stimulating editorial in the February issue of *The Review of Scientific Instruments*, Dr. G. P. Harnwell[1] has crystallized into a definite suggestion a feeling which has been growing for some time in the minds of many physicists that some concrete step must be taken to bring about greater unity among American physicists. A recent sampling of opinions,[2] taken by the American Physical Society of what should be done to produce greater participation in the affairs of the Society by physicists in industry, brought out almost unanimously the plea for improved means of exchanging ideas between the so-called academic physicists and industrial physicists. While the interests of some physicists may be concentrated in a relatively small part of the field of physics, nevertheless there are many physicists, particularly those in industry, whose interests are so broad that they find it necessary to maintain contact with several scientific and engineering societies and their publications, the fields of which frequently overlap. A strong central organization in the field of physics should help to correlate the various independent groups to the advantage of physics as a whole and should be able to provide for better organization in newly developing fields without the confusion and overlapping which might result if each society acted independently in an effort to cover new fields.

A diagram of the field of physics such as the one presented on the next page may serve to illustrate the relation of some of the member societies of the American Institute of Physics with respect to each other and to the field as a whole and also to indicate other possibilities which must be considered in any attempt to bring greater unity into the entire field of physics. The first five column headings in the diagram represent the five classical divisions in the field of physics. Perhaps all physics could be classed in these five columns or subdivisions of them, but for the purposes of this discussion some additional columns are added and still others might be. The first horizontal heading is "teaching" the success of which directly affects progress throughout the entire field. The other horizontal headings represent more or less logical stages from fundamental physics to applied physics. This diagram may be regarded as a map which could be called the "United States of Physics." The positions occupied by the Institute member societies are indicated and some overlapping of interests are apparent. Any consideration of the field of physics as a whole must include consideration of the various fields of applied physics which are now covered by established engineering societies, some of which are shown in the diagram. Whether or not the interests of these engineering societies should be limited to "application" or

[1] G. P. Harnwell, "A more perfect union," Rev. Sci. Inst. **15**, 19 (1944).
[2] "Current trends in the American Physical Society," J. App. Phys. **14**, 437 (1943).

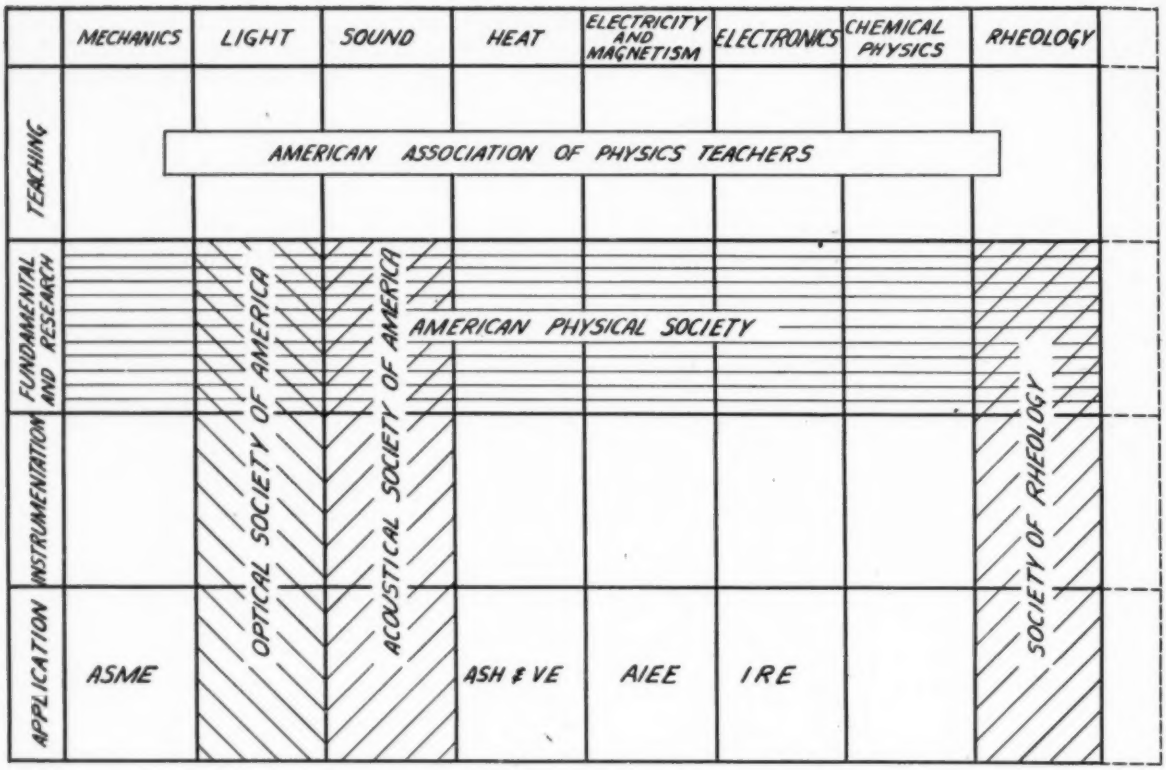

Diagram to illustrate the relation between the member societies of the American Institute of Physics to each other and to other related societies.

whether their interests extend up through the "instrumentation" and "research" squares is subject to debate. It is also apparent that in the fields of optics and acoustics there are two member societies of the Institute whose interests extend definitely into the field of "application."

If another diagram with the same vertical and horizontal headings is drawn and the subject matter covered by the Institute journals and member society journals is charted, overlapping is again apparent. Journals of some member societies and also *The Journal of Chemical Physics* attempt a full vertical coverage of the subjects of their interest while two of the societies publish journals covering teaching, fundamental physics, and research and the Institute publishes journals on instruments and applied physics which also provide horizontal coverage. Whether or not this overlapping is desirable or not is debatable. To some it may appear as undesirable competition; to others it will seem desirable since some physicists limit their interests primarily to one of the vertical divisions while others are interested primarily in a horizontal division such as teaching, research, or applications. To provide each of these groups with journals which have a sufficiently high percentage of interest to justify their subscription may require overlapping of the kind which now exists.

Further problems arise when groups of physicists interested in some special field organize, such as the recently formed American Society for X-Ray and Electron Diffraction and the Electron Microscope Society of America. Within the American Physical Society divisions of Electron and Ion Optics and of High Polymer Physics have been formed. Should such groups be encouraged to become divisions of one of the existing societies in physics and, if so, of which society, or should they form sovereign "states" and become a part of the "union"?

Obviously a strong central organization in physics is needed. A single society with many subject matter divisions or a "union" of many

"states" might accomplish the desired unity in physics provided the proper balance between "federal" power and "states' rights" is maintained. Each "state" could be autonomous in matters pertaining to meetings and publications in the field of interest. The power to handle problems affecting all physicists could be vested in the central organization. Possibly the "colonization" of virgin territory could best be left to the central organization rather than a matter for dispute among the "states."

The suggestions made above are provocative rather than conclusive. There is much food for thought in this imperialistic view of the field of physics. Perhaps no one central organization could hope to encompass the entire field. If the established engineering societies are not a part of the "union," they still are definitely on the "continent" of physics and "continental solidarity" demands that the closest of diplomatic relations be maintained with them.

The American Institute of Physics, through its member and affiliated societies, has a fair but not complete coverage of the field of physics, but it appears that a considerable modification of its present organization may be necessary to enable it to perform satisfactorily the functions of a strong central organization to unify physics. Traditions of individual societies may have to be broken. Compartmentalization of interests within the Institute, without unnecessary overlapping, should make for a strong and smooth working organization which would attract to it newly forming groups and older established groups which recognize their logical connection with physics. The promotion of joint meetings of societies and the publication of a journal devoted to no particular field but to the interests of the professional physicist, both pure and applied, would further aid in developing unity. Greater pride in and popular appreciation of the profession of physics should follow.

WALLACE WATERFALL
ELMER HUTCHISSON

"The presence of a great body of highly able scientific men in this country has recently been an indispensable asset in time of danger. We must be sure that it is again present if we are again threatened, and science of the highest type flourishes best when it seeks its own objectives and pursues its own uninhibited ways. If we perpetuate in this country in the years to come a scientific atmosphere and body of men of the caliber that we now have, I will fear no threat from any source, for in time of need they will again respond, they will again direct their full energies in a patriotic effort, working under a closely unified and controlled program of the application of science in the prosecution of war, and they will thus do their full part in the protection of this country."

DR. VANNEVAR BUSH, Director of the Office of Scientific Research and Development, in *Science*, December 31, 1943

Contributed Original Research

General Vibration of a Hinged Beam[1]

HERBERT KAPFEL BROWN
Rensselaer Polytechnic Institute, Troy, New York

(Received February 5, 1944)

This paper is a continuation of a paper by the author entitled "The Resolution of Boundary Value Problems by Means of the Finite Fourier Transformation: General Vibration of a String." A general boundary value problem of the transverse vibrations of a hinged beam was resolved into the solution of a pair of boundary value problems with much simpler boundary conditions. The finite sine transformation and its property of convolution were used to accomplish this. The transformed boundary value problem was solved by the introduction of a fundamental set of solutions of the homogeneous transformed problem.

BOUNDARY value problems which contain a partial differential equation of the fourth order with respect to the space variable can be resolved in certain cases (see Part III of G.V.S.) by means of the finite Fourier transformation. The determination of the vertical displacements of a hinged beam is a typical example.

It is to be understood that the presentation given here is heuristic; no claim of mathematical rigor is made.

1. GENERAL VIBRATION OF A HINGED BEAM

Consider a beam supported along its length by an elastic foundation. The resilience of the beam and the rigidity of the foundation may be functions of the time. An external force is applied along the beam parallel to the direction of transverse vibrations, while the ends $x=0$ and $x=\pi$ are subjected to arbitrary prescribed displacements and moments. The initial displacement of the beam and the initial velocity of points along the length of the beam are given also by prescribed functions.

The vertical displacements $V(x, t)$ of such a beam satisfy the following conditions in the region $R: 0<x<\pi,\ t>0$:

$$\begin{aligned} L(V)\equiv\frac{\partial^2}{\partial t^2}V+C_1(t)\frac{\partial^4}{\partial x^4}V \\ +C_2(t)\,V=P(x,t) \quad &\text{in } R, \\ V(+0,t)=C_3(t),\ V(\pi-0,t)=C_4(t) \quad &(t>0), \\ V_{xx}(+0,t)=C_5(t),\ V_{xx}(\pi-0,t)=C_6(t) \quad &(t>0), \\ V(x,+0)=F_1(x),\ V_t(x,+0)=F_2(x) \quad &(0<x<\pi), \end{aligned} \tag{A}$$

where the prescribed functions in this description satisfy the following conditions:

(a) F_1, F_2, P and their first four derivatives with respect to x vanish at the end points of the interval $(0, \pi)$.

(b) Since we do not want the beam to break or buckle at the end points of $(0, \pi)$ when t approaches zero, condition (a) demands that

$$C_i(0)=C_i'(0)=0 \quad (i=3, 4, 5, 6).$$

2. RESOLUTION OF BEAM PROBLEM

The method used in G.V.S. to express the transverse displacements of a vibrating string in terms of auxiliary functions, the solutions of simpler problems, can be used in this problem

[1] This paper is a continuation of the paper: Herbert K. Brown, "Resolution of boundary value problems by means of the finite Fourier transformation: general vibration of a string," J. App. Phys. **14**, 609–618 (1943). This paper will be referred to as G.V.S.

also. This method of solution of a problem is called the resolution of a problem into simpler problems, or simply the resolution of a problem.

The first step in the resolution of problem (A) is to express $V(x, t)$ as the sum of the solutions of seven boundary value problems which have the same differential expression $L(V)$, but which otherwise have simpler boundary conditions. That is, the sum

$$V(x, t) = \sum_{i=1}^{7} {}_iV(x, t) \tag{1}$$

satisfies all the conditions of problem (A), where ${}_iV(x, t)$ $(i=1, 2, \cdots, 7)$ are the solutions of the following seven problems:[2]

$$\left.\begin{aligned} L({}_1V) &= P(x, t) && \text{in } R,\\ M_1({}_1V) &= 0 && (t>0),\\ M_2({}_1V) &= 0 && (t>0),\\ N({}_1V) &= 0 && (0<x<\pi). \end{aligned}\right\} \tag{A$_1$}$$

$$\left.\begin{aligned} L({}_2V) &= 0 && \text{in } R,\\ {}_2V(+0, t) &= C_3(t), \\ {}_2V(\pi-0, t) &= 0 \end{aligned}\right\} \quad (t>0), \tag{A$_2$}$$

$$\left.\begin{aligned} M_2({}_2V) &= 0 && (t>0),\\ N({}_2V) &= 0 && (0<x<\pi). \end{aligned}\right\}$$

$$\left.\begin{aligned} L({}_3V) &= 0 && \text{in } R,\\ {}_3V(+0, t) &= 0, \\ {}_3V(\pi-0, t) &= C_4(t) \end{aligned}\right\} \quad (t>0), \tag{A$_3$}$$

$$\left.\begin{aligned} M_2({}_3V) &= 0 && (t>0),\\ N({}_3V) &= 0 && (0<x<\pi). \end{aligned}\right\}$$

$$\left.\begin{aligned} L({}_4V) &= 0 && \text{in } R,\\ M_1({}_4V) &= 0 && (t>0),\\ {}_4V_{xx}(+0, t) &= C_5(t), \\ {}_4V_{xx}(\pi-0, t) &= 0 \end{aligned}\right\} \quad (t>0), \tag{A$_4$}$$

$$N({}_4V) = 0 \qquad (0<x<\pi).$$

$$\left.\begin{aligned} L({}_5V) &= 0 && \text{in } R,\\ M_1({}_5V) &= 0 && (t>0),\\ {}_5V_{xx}(+0, t) &= 0, \\ {}_5V_{xx}(\pi-0, t) &= C_6(t) \end{aligned}\right\} \quad (t>0), \tag{A$_5$}$$

$$N({}_5V) = 0 \qquad (0<x<\pi).$$

$$\left.\begin{aligned} L({}_6V) &= 0 && \text{in } R,\\ M_1({}_6V) &= 0 && (t>0),\\ M_2({}_6V) &= 0 && (t>0), \\ {}_6V(x, +0) &= F_1(x), \\ {}_6V_t(x, +0) &= 0 \end{aligned}\right\} \quad (0<x<\pi). \tag{A$_6$}$$

$$\left.\begin{aligned} L({}_7V) &= 0 && \text{in } R,\\ M_1({}_7V) &= 0 && (t>0),\\ M_2({}_7V) &= 0 && (t>0), \\ {}_7V(x, +0) &= 0, \\ {}_7V_t(x, +0) &= F_2(x) \end{aligned}\right\} \quad (0<x<\pi). \tag{A$_7$}$$

The second step in the resolution of problem (A) is to apply the sine transformation to each of the problems (A_i) $(i=1, 2, \cdots, 7)$. However, since $V(x, t)$ can be written as the sum of the ${}_iV(x, t)$, the transform of $V(x, t)$ can be written as the sum of the transforms of the ${}_iV(x, t)$. So that, for convenience, as in the string problem, we apply the sine transformation to the original form of our problem, that is, problem (A), and obtain[3]

$$\left.\begin{aligned} \mathfrak{L}(v) \equiv v''(n, t) & \\ +[n^4C_1(t) + C_2(t)]v(n, t) &= q(n, t) \\ v(n, 0) = f_1(n), \quad v'(n, 0) &= f_2(n), \end{aligned}\right\} \tag{A'}$$

where

$$q(n, t) \equiv p(n, t) - C_1(t)[nC_5(t) - n^3C_3(t)].$$

Following the procedure of the string problem, we let $v_1(n, t)$ and $v_2(n, t)$ constitute a fundamental set of solutions of the homogeneous trans-

[2] (a) The expression $M_1({}_iV) = 0$ means that ${}_iV$ vanishes at both end points of the interval $(0, \pi)$. (b) The expression $M_2({}_iV) = 0$ means that ${}_iV_{xx}$ vanishes at both end points of the interval $(0, \pi)$. (c) The expression $N({}_iV) = 0$ means that the initial values of ${}_iV(x, t)$ and ${}_iV_t(x, t)$ are both zero.

[3] Since ${}_3V(x, t)$ and ${}_5V(x, t)$ can be expressed in terms of ${}_2V(x, t)$ and ${}_4V(x, t)$, respectively (see Note, p. 612, in G.V.S.), we can assume C_4 and C_6 to be identically zero, for the time being, which implies that ${}_3V$ and ${}_5V$ be identically zero also.

formed equation $\mathfrak{L}(v)=0$. We choose $v_1(n,t)$ and $v_2(n,t)$ so that the Wronskian[4] $\Delta(v_1, v_2)=1/n^2$; that is,

$$\mathfrak{L}(v_1)=0, \qquad \mathfrak{L}(v_2)=0,$$
$$v_1(n,0)=0, \quad (B_1') \qquad v_2(n,0)=1/n, \quad (B_2')$$
$$v_1'(n,0)=1/n, \qquad v_2'(n,0)=0.$$

The solution $v(n,t)$ of (A′) can be written

$$v(n,t)=f_1(n)nv_2(n,t)+f_2(n)nv_1(n,t)+\int_0^t q(n,\tau)nw(n,t,\tau)d\tau,$$

where, as in the string problem,

$$w(n,t,\tau)=v_1(n,t)v_2(n,\tau)-v_1(n,\tau)v_2(n,t).$$

The third step in the resolution of problem (A) is to express the transforms ${}_iv(n,t)$ of the ${}_iV(x,t)$ in terms of $v_1(n,t)$ and $v_2(n,t)$. This can be done at once; since when $q(n,\tau)$ is written in its expanded form, it is obvious that[3]

$$v(n,t)={}_1v+{}_2v+{}_4v+{}_6v+{}_7v,$$

where

$${}_1v(n,t)=\int_0^t p(n,\tau)n^2w(n,t,\tau)d\tau,$$

$${}_2v(n,t)=\int_0^t C_3(\tau)C_1(\tau)n^5w(n,t,\tau)d\tau,$$

$${}_4v(n,t)=-\int_0^t C_5(\tau)C_1(\tau)n^3w(n,t,\tau)d\tau,$$

$${}_6v(n,t)=f_1(n)nv_2(n,t),$$

$${}_7v(n,t)=f_2(n)nv_1(n,t).$$

Comparing these forms with (II-2.4) of G.V.S., we see that ${}_2v(n,t)$ is the only transform of the five which is essentially different from those discussed in the string problem.

3. INVERSION OF RESOLUTION

In expressing $v(n,t)$ as the solution of the transform of problem (A), that is, the solution of (A′), we introduced the transforms $v_1(n,t)$ and $v_2(n,t)$. The corresponding object functions $V_1(x,t)$ and $V_2(x,t)$ satisfy the following conditions in the region R: $0<x<\pi$, $t>0$:

$$\left.\begin{aligned} L(V_1)&=0 && \text{in } R,\\ M_1(V_1)&=0 && (t>0),\\ M_2(V_1)&=0 && (t>0),\\ V_1(x,+0)&=0,\\ V_{1t}(x,+0)&=\frac{\pi-x}{\pi} && (0<x<\pi). \end{aligned}\right\} \quad (B_1)$$

$$\left.\begin{aligned} L(V_2)&=0 && \text{in } R,\\ M_1(V_2)&=0 && (t>0),\\ M_2(V_2)&=0 && (t>0),\\ V_2(x,+0)&=\frac{\pi-x}{\pi},\\ V_{2t}(x,+0)&=0 && (0<x<\pi). \end{aligned}\right\} \quad (B_2)$$

All of the inversion forms of $w(n,t,\tau)$ which were developed in the string problem can be duplicated here, excepting, of course, the expression which involves the partial differential equation of the homogeneous string problem. Instead, $W(x,t,\tau)$, the inverse of $w(n,t,\tau)$, has several additional properties, including the particular transform

$$\begin{aligned} n^4w(n,t,\tau)&=n^4v_1(n,t)v_2(n,\tau)-n^4v_1(n,\tau)v_2(n,t)\\ &=\mathfrak{S}\left\{\frac{\partial^4}{\partial x^4}V_1(x,t)\right\}\mathfrak{S}\{V_2(x,\tau)\}\\ &\quad-\mathfrak{S}\left\{\frac{\partial^4}{\partial x^4}V_1(x,\tau)\right\}\mathfrak{S}\{V_2(x,t)\}\\ &=\mathfrak{C}\left\{-\frac{1}{2}\frac{\partial^4}{\partial x^4}V_1(x,t)*V_2(x,\tau)\right.\\ &\quad\left.+\frac{1}{2}\frac{\partial^4}{\partial x^4}V_1(x,\tau)*V_2(x,t)\right\}\\ &=\mathfrak{C}\left\{\frac{\partial^4}{\partial x^4}W(x,t,\tau)\right\}, \end{aligned}$$

where, by Faltung theorem III of G.V.S.,

$$W(x,t,\tau)=-\tfrac{1}{2}\int_{-\pi}^{\pi}[V_1(x-\xi,t)V_2(\xi,\tau)-V_1(x-\xi,\tau)V_2(\xi,t)]d\xi,$$

[4] $\Delta(v_1,v_2)\equiv[v_1'(n,t)v_2(n,t)-v_1(n,t)v_2'(n,t)]$.

where both V_1 and V_2 are defined as the odd and periodic extensions of the original functions V_1 and V_2.

The final step in the resolution of problem (A) is the inversion of the transforms ${}_iv(n, t)(i=1, 2, 4, 6, 7)$. We need to consider only the transform

$$
\begin{aligned}
{}_2v(n, t) &= \int_0^t C_3(\tau)C_1(\tau)n^5 w(n, t, \tau)d\tau \\
&= \int_0^t C_3(\tau)C_1(\tau)n\mathfrak{C}\left\{\frac{\partial^4}{\partial x^4}W(x, t, \tau)\right\}d\tau \\
&= -\int_0^t C_3(\tau)C_1(\tau)\mathfrak{S}\left\{\frac{\partial^5}{\partial x^5}W(x, t, \tau)\right\}d\tau.
\end{aligned}
$$

Therefore, assuming that we can interchange the order of the operations of integration and sine transformation, we have that

$$
{}_2V(x, t) = -\int_0^t C_3(\tau)C_1(\tau)\frac{\partial^5}{\partial x^5}W(x, t, \tau)d\tau. \quad (2)
$$

The remaining four transforms ${}_1v(n, t)$, ${}_4v(n, t)$, ${}_6v(n, t)$, and ${}_7v(n, t)$ have inversions which can be tabulated from (II-3) of G.V.S. as follows:

$$
\begin{aligned}
{}_1V(x, t) &= -\tfrac{1}{2}\int_0^t\int_{-\pi}^{\pi} P(x-\xi, \tau)W_{\xi\xi}(\xi, t, \tau)d\xi d\tau, \\
{}_4V(x, t) &= -\int_0^t C_5(\tau)C_1(\tau)W_{xxx}(x, t, \tau)d\tau, \\
{}_6V(x, t) &= \tfrac{1}{2}\int_{-\pi}^{\pi} F_1(x-\xi)V_{2\xi}(\xi, t)d\xi, \\
{}_7V(x, t) &= \tfrac{1}{2}\int_{-\pi}^{\pi} F_2(x-\xi)V_{1\xi}(\xi, t)d\xi.
\end{aligned} \quad (3)
$$

Further, we have from ${}_2V(x, t)$ and ${}_4V(x, t)$ that

$$
{}_3V(x, t) = \int_0^t C_4(\tau)C_1(\tau)\frac{\partial^5}{\partial x^5}W(\pi-x, t, \tau)d\tau,
$$

and

$$
{}_5V(x, t) = \int_0^t C_6(\tau)C_1(\tau)W_{xxx}(\pi-x, t, \tau)d\tau.
$$

According to Eqs. (1), (2), and (3), the solution of problem (A) is given in terms of the solutions V_1 and V_2 of the problems (B_1) and (B_2), respectively, as follows:

$$
\begin{aligned}
V(x, t) = &-\tfrac{1}{2}\int_0^t\int_{-\pi}^{\pi} P(x-\xi, \tau)W_{\xi\xi}(\xi, t, \tau)d\xi d\tau \\
&-\int_0^t C_3(\tau)C_1(\tau)\frac{\partial^5}{\partial x^5}W(x, t, \tau)d\tau \\
&+\int_0^t C_4(\tau)C_1(\tau)\frac{\partial^5}{\partial x^5}W(\pi-x, t, \tau)d\tau \\
&-\int_0^t C_5(\tau)C_1(\tau)W_{xxx}(x, t, \tau)d\tau \\
&+\int_0^t C_6(\tau)C_1(\tau)W_{xxx}(\pi-x, t, \tau)d\tau \\
&+\tfrac{1}{2}\int_{-\pi}^{\pi} F_1(x-\xi)V_{2\xi}(\xi, t)d\xi \\
&+\tfrac{1}{2}\int_{-\pi}^{\pi} F_2(x-\xi)V_{1\xi}(\xi, t)d\xi.
\end{aligned} \quad (4)
$$

The transverse vibration problem (A) with general boundary conditions is thus resolved by formula (4) into the solution of a pair of problems (B_1) and (B_2) with much simpler boundary conditions.

The Effect of Thixotropy on Plasticity Measurements

HENRY GREEN AND RUTH N. WELTMANN
Interchemical Corporation, New York, New York
(Received February 3, 1944)

THE rheological measurement of a thixotropic system presents two outstanding problems. First, how to measure the magnitude of the thixotropic phenomenon; second, how to designate the particular state of structural breakdown in which the material exists at the moment of measurement.

It is possible to visualize two extremes: one where no thixotropic breakdown has occurred; the other, where the breakdown is complete. Breakdown arises from agitation or stirring such as occurs in viscometers; consequently, the material, when subjected to viscometric measurement, will be either in a complete or in a partial state of thixotropic breakdown. In actual practice this state is far more likely to be partial than complete; hence the necessity for designating it. This is particularly true for materials like printing inks, paints, and pigment vehicle suspensions in general.

The authors have published papers[1–3] showing how these problems can be investigated by means of the thixotropic hysteresis loop. So far their articles have been concerned mainly with developing the theory and equations of the loop. The present paper will be devoted to laboratory procedures, that is, to a process whereby plastic viscosity and yield value can be recorded at a known "thixotropic level;" and the coefficients of thixotropic breakdown calculated.

THE CONSISTENCY FACTORS

Plastic Viscosity, *U*

This is a term[1] employed in place of the "reciprocal of mobility." In *non-thixotropic* plastics the value of U is constant, being independent of the rate of shear. It is necessary to point this out so that U will not be confused with the so-called "apparent viscosity." The concept of apparent viscosity is not used by the authors in any of their papers. In *thixotropic* materials the plastic viscosity decreases with agitation in accordance with certain rules explained below. When the material is flowing (being stirred) the qualifying term "dynamic" is sometimes used in conjunction with U and f.

Yield Value, *f*

In non-thixotropic plastics the concept of yield value is easily visualized. With thixotropic materials the subject becomes more complex. There is sufficient evidence in such cases to indicate that yield value in the static state is greater than dynamic yield value. However, the smallest yield value intercept is obtained with the smallest top rate of shear and increases with increasing top rate of shear. See Fig. 1. T_2 is the yield value intercept.

Thixotropic Level

Except for the lower end, the down curve side of the hysteresis loop is linear. This straight line relationship indicates a thixotropic stability or "thixotropic level." Hence, since stability can be maintained long enough to obtain a straight flow curve, both yield value and plastic viscosity can be determined. Since the position of the down curve depends on the top angular velocity employed, the particular state of structural break-

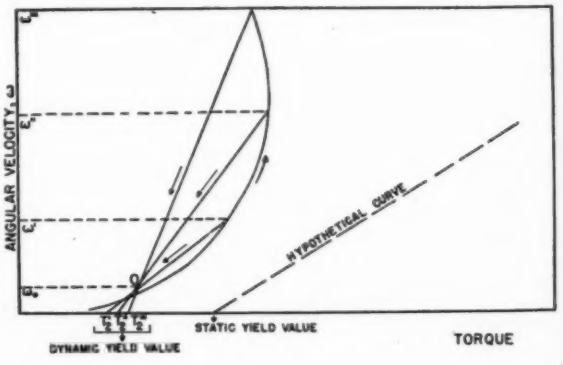

FIG. 1.

[1] Henry Green, Ind. Eng. Chem. Anal. Ed. **14**, 576 (1942).
[2] H. Green and R. N. Weltmann, Ind. Eng. Chem. Anal. Ed. **15**, 201 (1943).
[3] Ruth N. Weltmann, J. App. Phys. **14**, 343 (1943).

down or thixotropic level can be designated by giving the velocity gradient at this highest point. The velocity gradient is calculated for the position midway between the bob and cup, when a rotational viscometer is used. It is preferable that this distance be as small as conveniently possible. This is explained more in detail below.

The Coefficients of Thixotropic Breakdown

It would be ideal if the thixotropic magnitude could be expressed by a single quantity. Goodeve and Whitfield[4] claim to have accomplished this. By an ingenious process of deduction they arrive at the conclusion that the intercept on the force axis formed by the straight part of the consistency curve is the "coefficient of thixotropy." Their conclusion, so far, has not been refuted. However, Pryce-Jones[5] points out the impossibility of measuring thixotropy from a single consistency curve, which complies entirely with our own ideas. Furthermore, it is possible to have two plastic materials showing the same intercept but behaving differently upon stirring. One might break down thixotropically while the other might show no visible sign of change in consistency. An analysis of the hysteresis loop gives two coefficients, M and V, of thixotropic breakdown, V being zero in those cases where f does not change with U.[6] A coefficient B relating breakdown with time has also been derived. These coefficients are defined as follows:

1. A coefficient, designated by the symbol M, which is the loss in shearing force per unit area per unit increase in velocity gradient.[2] 2. A coefficient designated by the symbol V, which gives the change in yield value per unit change in plastic viscosity.[6] 3. A coefficient designated by the symbol B, which is the product of the rate of decrease in plastic viscosity times the length of time the breakdown force is applied.[3]

THE VISCOMETER

The viscometer, Fig. 2, used for producing the hysteresis loop has been described in detail elsewhere.[1] It is the rotational type in which the distance between the cup and bob is sufficiently small to give satisfactory linear down curves for plastic materials. The viscometer is further constructed so that rapid changes can be made in the rotation of the cup. The customary phosphor-bronze wires from which the bob is usually suspended are replaced by helical steel springs ranging from ones giving slight torsion to those that are difficult and hard to twist. The bob is fastened to a stout shaft which is held centered by two sets of ball bearings. The r.p.m. can be varied from 5 to 400. The apparatus is capable of giving consistency curves covering materials with viscosities from 1 to 2500 poises and yield values up to 180,000 dynes/cm^2. Materials like printing inks fall within this range.

FIG. 2.

A. Calibration

The springs are calibrated directly by weights and not by using liquids of known viscosities. This can be done because of the ball-bearing support received by the bob shaft. The advantage is that heavy oils (of uncertain viscosity) need not be employed in calibrating the stiffest springs. The weights are suspended from a string, which, after passing over a pulley wheel, is fastened to the horizontal disk containing the torsion scale. This disk is firmly attached to the bob shaft. In this manner the suspended weight exerts a torque and causes the bob and spring to twist through a measurable number of degrees of arc. The torsion

[4] C. F. Goodeve and G. W. Whitfield, Trans. Faraday Soc. **34**, 511 (1938).
[5] J. Pryce-Jones, J. Oil Colour Chem. Assoc. **19**, 293 (1926).
[6] H. Green and R. N. Weltmann, to be published.

constant of the spring is the product of the weight in grams times the acceleration due to gravity times the radius of the disk divided by the degrees of deflection.

B. Centering the Bob

In order to prevent the material under test from riding out of the cup during rotation, it is necessary that the bob be exactly centered with respect to the cup axis. The viscometer is so constructed that the entire head holding the bob can be moved laterally while the cup is rotating. If the bob is off center during rotation, any liquid that is in the cup will overflow at the narrowest distance between the bob and the cup. By moving the bob backward and forward, a position can be found where no further overflow takes place. The head of the viscometer is then firmly clamped in place at this position. In addition, a cover, the inner edge of which nearly touches the bob, is fitted on the cup to secure further the material from riding out.

C. Filling the Cup

In order to get linear down curves (except at the extreme lower end) it is essential that no air bubbles be accidently trapped in the material while the bob is being lowered into the cup. If the material is the type of substance that is capable of forming a skin over its surface (such as printing inks and paints), care must be taken that no skin is included in the sample.

D. Temperature Control

The viscometer employed by the authors operates in a water bath, the temperature of which is controlled to $\pm 0.2°C$. After the bob has been lowered into the cup a period of about 20 minutes is required for the sample to reach temperature. The up curve is then commenced.

THE PROCEDURE

A. Obtaining the Loop

The lowest r.p.m. that can be used conveniently on the instrument is approximately 5. About 15 increases in r.p.m. are made in obtaining the up curve side of the loop; the same number of decreases are made in getting the down curve side. These changes are made in intervals spaced as evenly as possible both in regard to the number of r.p.m. and to time. The change in r.p.m. is accomplished by a Graham continuously variable transmission and gives a top speed of about 400 r.p.m. The change is made without stopping the rotation of the cup and in steps as small or as large as desired. The top r.p.m. will be capitalized, R.P.M.

B. Calculating U

The plastic viscosity U is determined from the cotangent of the angle formed by the torque axis and the linear portion of the down curve. The equation for doing this is derived from the Reiner and Riwlin[7] equation of flow for rotational viscometers:

$$U=\frac{(T-T_2)S}{\omega}, \tag{1}$$

where T is the torque, T_2 the intercept, $S=[(1/R_b^2)-(1/R_c^2)]/4\pi h$, R_b being the radius of the bob, R_c the radius of the cup, and h the height of the bob.

C. Calculating f

The yield value in dynes/cm^2 is obtained by multiplying the torque intercept T_2 by a constant of the apparatus. This constant is also obtained from the Reiner and Riwlin equation.

$$f=CT_2, \tag{2}$$

where $C=S/\ln(R_c/R_b)$.

D. The Velocity Gradient

The speed with which one layer of a thixotropic material flows past its adjacent layer evidently must be the dominant factor involved in its breakdown. This speed is not properly expressed by top r.p.m. or ω. It can be definitely designated, however, by the top velocity gradient or rate of shear, dv/dr. For any r.p.m. the rate of shear varies from the wall of the bob to the wall of the cup. Its maximum value is at the wall of the bob. If the radii of the cup and bob are sufficiently large and the difference between them is kept small, then the decrease in the velocity gradient

[7] M. Reiner and R. Riwlin, Kolloid Zeits. **43**, 1 (1927).

from bob to cup is practically linear. Also, data have been published showing that thixotropic breakdown varies linearly with the velocity gradient.[2] Therefore it is justifiable to assume that the average breakdown takes place at the midpoint between cup and bob. In other words, the amount of breakdown in excess of the average taking place at the wall of the bob is offset by an equal deficiency in breakdown at the wall of the cup. In Table I are shown the dimensions of four

TABLE I. Velocity gradients for different viscometers.

Viscom.	R_c, cm	R_b, cm	$R_c - R_b$	dv/dr at midpoint (1 r.p.m.)	% drop in dv/dr bob to cup
1	1.50	1.30	0.20	0.719	25.0
2	1.40	1.30	0.10	1.40	13.7
3	2.00	1.95	0.05	3.67	5.0
4	5.16	5.01	0.15	3.58	5.6

of our viscometers together with the velocity gradients per r.p.m.; also the percentage drop in dv/dr from bob to cup. The relationship between dv/dr at the midpoint and r.p.m. is as follows:

$$(dv/dr)_{\text{mid}} = (\text{r.p.m.})/15hS(R_c+R_b)^2. \quad (3)$$

E. Calculating U for Interpolated Values of Top r.p.m.

It is often desirable to know the value of U for a top r.p.m. other than that employed in the original measurement. Such a determination can be made, if two values of U are known for two different top r.p.m. These values of U and R.P.M. must be obtained from a series of loops that have the same time element in common, such as shown in Fig. 1, ω', ω'', etc. By "time element," or later on simply "time," is meant the time interval during which the shearing force is allowed to operate for each experimental point. This interval is a constant throughout the length of any one up curve.[2]

It has been shown experimentally[2] that when the change in f is negligible, the curve U *vs.* $\ln[1/(\text{R.P.M.})^2]$ is linear. (See Fig. 3.) However, when the change in f is appreciable it follows by deduction (depending on assumptions in regard to the crossing point discussed in Section G) that a straight line relation can be had only if U is plotted against $\ln[1/(\text{R.P.M.}-\text{R.P.M.}_0)^2]$ (R.P.M.$_0$ corresponding to ω_0 in

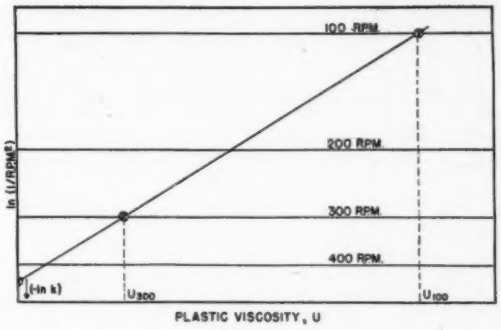

FIG. 3.

Fig. 1). Fortunately the omission of the relatively small R.P.M.$_0$ does not affect the linearity of the curve to a detectable extent, even though it does shift its position. Consequently, whether f changes or not, satisfactory interpolated values of U can still be had from the curve as plotted in Fig. 3.

For practical purposes the curve in Fig. 3 can be obtained from a single U, R.P.M., and loop area A. It has been shown that[2]

$$mU = \ln(k/\omega^2) \quad (4)$$

and

$$m = \omega^2/2AS. \quad (5)$$

Equation (5) and the above statement, however, hold theoretically and experimentally only when the up curve is run so rapidly that thixotropic breakdown arising from the time factor is negligible. A theoretical curve like this has been described previously by the authors.[2] Actually it is impossible to obtain such an ideal loop by experimental means; but an up curve comprised of 15 points run in less than two minutes (by the procedure described in this paper) has been found to approximate the ideal curve sufficiently for practical purposes. This can be demonstrated by comparing the value of m obtained experimentally from Eq. (5) with values obtained by methods independent of time. Refer to Eq. (8). Note that $m = 2/M$. From Eqs. (4) and (5) it follows that the intercept (Fig. 3) is

$$-\ln k = \ln\left[1\Big/\left(\frac{\text{R.P.M.}}{9.55}\right)^2\right] - U(\text{R.P.M.}/9.55)^2/2AS, \quad (6)$$

where R.P.M./9.55 $=\omega$. With the intercept

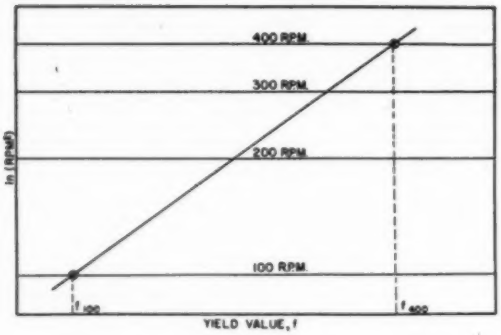

FIG. 4.

known and one other point, say U at 100 r.p.m., the curve in Fig. 3 can be drawn.

The loop area is measured with a planimeter. If the planimeter gives results in square inches z, then this value must be changed to comply with the dimensions of A in Eq. (6). Assume that the loop has been formed by plotting r.p.m. *vs.* torque. Let 1 inch on the r.p.m. axis be equal to x r.p.m.; and 1 inch on the torque axis equal to y dynes cm of torque. Then the values of A in dynes cm/sec. will be xyz.

The procedure of obtaining interpolated values of U is extremely important in the measurement of printing inks. The tack or "pull-resistance"[8] of the ink varies with U, which, in turn, depends on the speed of the printing press, because printing inks are thixotropic.

F. Calculating f for Interpolated Values of Top r.p.m.

Because f varies with the top r.p.m., it is desirable to obtain interpolated values of f in a manner similar to the method used for U. If the same assumptions are made here as in Section E, it follows that the relation f *vs.* ln (R.P.M. $-$R.P.M.$_0$)^2 should be linear. Again, R.P.M.$_0$ being relatively small its omission, while affecting the position of the curve, does not show any detectable results on its linearity; consequently the omission can be made and the curve plotted and used as shown in Fig. 4.

G. The Coefficients of Thixotropic Breakdown

As pointed out, an analysis of the loop gives no coefficient defining thixotropic magnitude. It does show how thixotropic breakdown can be expressed in terms of changes induced in U and f by the application of velocity gradient and time. For practical purposes it can be assumed that the down curves, Fig. 1, cross at a common point, 0; also, it can be assumed that the up curve passes through this same point. Neither of these assumptions is strictly true; but this is the only basis, at present, upon which a theoretically derived expression for thixotropic breakdown can be obtained from the loop. When the above assumptions are made, it can be shown that a theoretical value V exists which must be a constant for the material under test, and gives the change in yield value with respect to the change in plastic viscosity.[6] The value of V is:

$$V=(f_2-f_1)/(U_1-U_2). \tag{7}$$

V is determined experimentally from two yield values and their corresponding plastic viscosities; V can be derived also by dividing the slope of the curve in Fig. 3 by the slope of the curve in Fig. 4. Experimentally both these curves appear to be linear; V therefore is apparently constant and the assumptions from which V is derived cannot be very far from the truth. The slopes of both curves can be shown experimentally to be independent of time;[6] hence V must be independent of time.

In the more elementary cases where the change in f is negligible, M is the only coefficient of thixotropic breakdown arising from increase in velocity gradient. This coefficient is likewise independent of time. It can be derived experimentally from two down curves where the time element is the same for both.

$$M=2(U_1-U_2)/\ln(\omega_2^2/\omega_1^2). \tag{8}$$

A time coefficient of thixotropic breakdown can also be obtained.[3] This gives the relation between breakdown and the total length of time employed in producing the breakdown. When the same top r.p.m. is used and a series of down curves is run after this top shearing force has been applied for different lengths of time t, then a straight line relation occurs when U is plotted against ln t.

$$B=-dU/d\ln t=-(dU/dt)t. \tag{9}$$

[8] Henry Green, Ind. Eng. Chem. Anal. Ed. **13**, 632 (1941).

By integrating between limits

$$B=(U_2-U_1)/(\ln t_1-\ln t_2). \qquad (10)$$

In order to determine B, it is necessary, then, to obtain the plastic viscosities from two down curves, each starting from the same top r.p.m., together with their respective time intervals. The time is measured from the moment the inertial effect of the bob has subsided until the down curve is commenced.

CONCLUSION AND SUMMARY

It is apparent from what has preceded that the effect of thixotropic breakdown on rheological measurement is to shift the position of the flow curve. It is quite impossible to say that this shift is a certain percentage of the total distance between the consistency of the untouched material and that of the material after complete breakdown has ensued. Such a method would be untenable for two reasons. First, plastic viscosity cannot be determined without forcing the material to flow; in which case the material is no longer "untouched." Second, there is no way of knowing when a completely broken down state is finally attained.

In view of these unsurmountable difficulties a different approach to the problem must be had. From a practical laboratory viewpoint there is only one reason why it is desirous to know the particular point in the scale of thixotropic breakdown where measurement has been made, and that is so measurements can be duplicated whenever required. This concept presents us with a relatively easy method for solving the problem. It has been shown that no breakdown takes place in forming the down curve of the loop when the loop is produced with a rotational viscometer. It has also been demonstrated that the position of the down curve depends on the top velocity gradient and the length of time of its application. In a suitably constructed rotational viscometer the velocity gradient can be adjusted to the desired value by selecting the correct top r.p.m.; and the time of application can be measured with a stopwatch. Thus a method becomes available for controlling and duplicating the energy used in producing breakdown.

The question that now arises is: Will a thixotropic material which receives the same treatment in regard to rate of shear and time of application always attain the same thixotropic level? The answer to the question presented in that manner is, naturally, No. It is obvious that if a material is given to an investigator for measurement at different thixotropic levels, the measurements are not necessarily going to check if the same top r.p.m. is used. It is necessary that the material be properly conditioned so that measurements are started always from the same level.

The ideal method of conditioning would be to allow the material to remain undisturbed until it attained its maximum structural growth. This should be carried out in the viscometer cup with the bob inserted. Unfortunately such a procedure is not likely to be practical for it would tie up the use of the viscometer for a day or even longer. In factory control work this would be prohibitive.

TABLE II. Measurements made by different operators using different viscometers.

Thixotropic material	Operator	Viscometer	Sample	U, poises	f, dynes/cm²
1	1	1	1	110	690
	2	2	1	117	735
	3	3	1	106	690
	4	4	1	104	795
	5	5	1	108	670
	6	6	1	111	690
2	1	1	1	95.2	1070
	2		2	98.0	980
	3		3	95.0	1070
	4		4	97.0	930
	5		5	96.0	1020
3	1	1	1	350	5700
	2		2	360	4900
	3		3	365	6700
4	1	1	1	170	13500
	2		2	176	12900
	3		3	178	13600
5	1	1	1	98.0	2850
	2		2	98.0	2800
	3		3	98.0	2800
6	1	1	1	560	23000
	2		2	563	26000
7	1	1	1	760	12200
	2		2	800	12200
8	1	1	1	156	600
	2		2	145	500

The next best method is to "age" the material in its own container. During the subsequent transference from container to cup some damage to the thixotropic structure is unavoidable; however, this damage is done at what would be equivalent to relatively low rates of shear. The percentage drop in plastic viscosity is small here in comparison with the percentage decrease resulting from a top r.p.m. of 100 or more; consequently breakdown will continue when the velocity gradient is further increased above the low rates of shear, and the position of the final level will have been affected very little if at all. This conclusion becomes obvious when it is realized that points at the lower end of the consistency curve can never be determined with precision; and when these points fall noticeably from the curve the main or upper part of the curve is apparently not affected as a result.

A study of the attached laboratory data will demonstrate the practical value of that fact. No standardized method can be developed for removing a thixotropic material from its container so that it can be put into the viscometer in such a way that the same amount of breakdown will always occur. Therefore, if various investigators attempted to measure different samples of the same thixotropic substance they would commence measurement on materials that had received different initial treatments corresponding to different low rates of shear; yet if they all commence their down curves at the same top dv/dr they can check one another. The greater the difference between the top rate of shear and the low rate of shear due to handling, the better the chance of checking. In Table II are shown the experimental results obtained by six investigators using six different viscometers. Each was given the same materials for measurement and all measurements on each material were made on the same day, thus ensuring equal aging. No instructions were given as to the exact manner in which the material was to be transferred from container to viscometer, each investigator using his own judgement in the matter. The checks are close and indicate that any difference in handling that occurred did not substantially affect the results.

ACKNOWLEDGMENT

The authors express their thanks to Interchemical Corporation for permission to publish this paper and to Evelyn Berezin for assistance with the laboratory work.

Development of the General Antenna Array Equation

WILLIAM T. THOMSON
Cornell University, Ithaca, New York

(Received November 12, 1943)

Interference patterns resulting from a system of orderly arranged sources, whether they be radio, light, or sound waves, can be conveniently analyzed by the use of the exponential operator e^{j}. This paper illustrates the application of the exponential operator in the development of the equation for the general antenna array.

INTRODUCTION

DIRECTIVE antennas are used rather generally for station-to-station communication, resulting at the transmitting end in a substantial reduction of the necessary power, and at the receiving end in an improvement in the ratio of signal to noise. In many instances interference between stations may also be avoided. In literature dealing with the subject, reference is often made to the general equation for the directive antenna array developed by G. C. Southworth.[1,2] The purpose of this paper is to present an alternate and somewhat simpler

[1] G. C. Southworth, Bell Tech. J. **10**, No. 1 (January, 1931); Proc. I.R.E. **18**, 1502 (1930).
[2] See F. E. Terman, *Radio Engineering*, second edition, p. 688 (1937).

derivation of the same equation by the use of exponential operators.

DERIVATION OF EQUATION

The sources comprising the general antenna array are considered equispaced and equiphased along each of the three rectangular coordinates. Using the same notation as Southworth, the coordinates of each element will be specified with letters n, N, N along the x, y, z axes, respectively. The source at the origin will be designated as $n, N, N=(1, 1, 1)$. (See Fig. 1.) The spacing along the x, y, z axes will be specified as $a\lambda$, $A\lambda$, and $A\lambda$, respectively.

Consider a wave in the direction θ, ϕ as shown in Fig. 1, and pass a plane perpendicular to the radius vector passing through the particular element in consideration. Using the origin as reference the space phase becomes equal to the distance from the origin to the plane measured along the radius vector; e.g.,

$$\psi_{211}=\frac{2\pi}{\lambda}(a\lambda\cos\phi\sin\theta)=2\pi a\cos\phi\sin\theta=\psi_x,$$

$$\psi_{311}=\frac{2\pi}{\lambda}(2a\lambda\cos\phi\sin\theta)=4\pi a\cos\phi\sin\theta$$
$$=2\psi_{211}=2\psi_x,$$

$$\psi_{121}=\frac{2\pi}{\lambda}(A\lambda\sin\phi\sin\theta)=2\pi A\sin\phi\sin\theta=\psi_y,$$

$$\psi_{112}=\frac{2\pi}{\lambda}(A\lambda\cos\theta)=2\pi A\cos\theta=\psi_z.$$

If the time phase between adjacent elements along the x, y, z is $(2\pi/\lambda)(b\lambda)$, $(2\pi/\lambda)(B\lambda)$, $(2\pi/\lambda)(B\lambda)$, respectively, the total phase along each axis becomes:

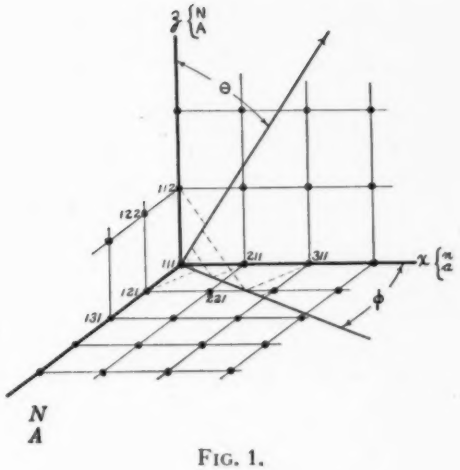

FIG. 1.

$$\psi(x)=2\pi(a\cos\phi\sin\theta+b),$$
$$\psi(y)=2\pi(A\sin\phi\sin\theta+B), \qquad (1)$$
$$\psi(z)=2\pi(A\cos\theta+B).$$

The field strength at a distant point in the θ, ϕ direction is the sum of the voltages due to each source in their proper phase relation. The difference in phase of each source is conveniently accounted for by the introduction of the exponential operator e^j, operating on a unit vector. Thus $e^{j\psi}=\cos\psi+j\sin\psi$ represents an operation in which the unit vector is rotated through an angle ψ, and the sum of two unit vectors differing by a phase angle ψ is $(1+e^{j\psi})$.

Designating the field strength of each source to be E_0, and taking all elements in the xy plane, we have

$$\begin{aligned}
E_{xy}=E_0\{&1+e^{j\psi(x)}+e^{2j\psi(x)}+\cdots e^{(n-1)j\psi(x)} && \text{along } x \text{ axis } (N=1)\\
&+e^{j\psi(y)}+e^{j[\psi(x)+\psi(y)]}+e^{j[2\psi(x)+\psi(y)]}+\cdots e^{j[(n-1)\psi(x)+\psi(y)]}] && \text{along } N=2\\
&+e^{2j\psi(y)}+\cdots && \text{along } N=3\\
&\vdots\\
&+e^{j(N-1)\psi(y)}+\cdots e^{j[(n-1)\psi(x)+(N-1)\psi(y)]}\}\\
=E_0\{&[1+e^{j\psi(x)}+e^{2j\psi(x)}+e^{3j\psi(x)}+\cdots e^{j(n-1)\psi(x)}]1\\
&+[1+e^{j\psi(x)}+e^{2j\psi(x)}+e^{3j\psi(x)}+\cdots e^{j(n-1)\psi(x)}]e^{j\psi(y)}\\
&+[1+e^{j\psi(x)}+e^{2j\psi(x)}+e^{3j\psi(x)}+\cdots e^{j(n-1)\psi(x)}]e^{2j\psi(y)}\cdots, \text{ etc.}\}\\
=E_0\{&[1+e^{j\psi(x)}+e^{2j\psi(x)}+\cdots e^{j(n-1)\psi(x)}][1+e^{j\psi(y)}+e^{2j\psi(y)}+\cdots e^{j(N-1)\psi(y)}]\}. \qquad (2)
\end{aligned}$$

The effect of each element in the plane above (e.g., $N=2$) can be obtained by multiplying each term in the x y plane by $e^{j\psi(z)}$ and the effect of the next plane (e.g., $N=3$) by multiplying each term of the x y plane by $e^{2j\psi(z)}$, etc.

The total voltage can then be obtained as:

$$\begin{aligned}E_T = E_0\{&[1+e^{j\psi(x)}+e^{2j\psi(x)}+\cdots][1+e^{j\psi(y)}+e^{2j\psi(y)}+\cdots]1\\&+[1+e^{j\psi(x)}+e^{2j\psi(x)}+\cdots][1+e^{j\psi(y)}+e^{2j\psi(y)}+\cdots]e^{j\psi(z)}\\&+[1+e^{j\psi(x)}+e^{2j\psi(x)}+\cdots][1+e^{j\psi(y)}+e^{2j\psi(y)}+\cdots]e^{2j\psi(z)}\cdots\}\\=E_0&[1+e^{j\psi(x)}+e^{2j\psi(x)}+\cdots e^{(n-1)j\psi(x)}][1+e^{j\psi(y)}+e^{2j\psi(y)}+\cdots e^{(N-1)j\psi(y)}][1+e^{j\psi(z)}+\cdots e^{(N-1)j\psi(z)}]. \quad (3)\end{aligned}$$

Each of the brackets is a geometric progression.

$$\therefore \quad E_T = E_0\left\{\frac{1-e^{nj\psi(x)}}{1-e^{j\psi(x)}}\right\}\left\{\frac{1-e^{Nj\psi(y)}}{1-e^{j\psi(y)}}\right\}\left\{\frac{1-e^{Nj\psi(z)}}{1-e^{j\psi(z)}}\right\}. \quad (4)$$

Substituting

$$(1-e^{nj\psi}) = (1-\cos n\psi) - j\sin n\psi,$$

$$|1-e^{nj\psi}| = [(1-\cos n\psi)^2+\sin^2 n\psi]^{\frac{1}{2}}$$

$$= \sqrt{2}(1-\cos n\psi)^{\frac{1}{2}} = \sqrt{2}\left(2\sin^2\frac{n\psi}{2}\right)^{\frac{1}{2}} = 2\sin\frac{n\psi}{2},$$

$$E_T = E_0\left\{\frac{\sin\dfrac{n\psi_{(x)}}{2}}{\sin\dfrac{\psi_{(x)}}{2}}\right\}\left\{\frac{\sin\dfrac{N\psi_{(y)}}{2}}{\sin\dfrac{\psi_{(y)}}{2}}\right\}\left\{\frac{\sin\dfrac{N\psi_{(z)}}{2}}{\sin\dfrac{\psi_{(z)}}{2}}\right\}. \quad (5)$$

Substituting values for ψ from (1),

$$\begin{aligned}E_t = E_0&\left\{\frac{\sin n\pi(a\cos\phi\sin\theta+b)}{\sin\pi(a\cos\phi\sin\theta+b)}\right\}\\&\times\left\{\frac{\sin N\pi(A\sin\phi\sin\theta+B)}{\sin\pi(A\sin\phi\sin\theta+B)}\right\}\\&\times\left\{\frac{\sin N\pi(A\cos\theta+B)}{\sin\pi(A\cos\theta+B)}\right\}, \quad (6)\end{aligned}$$

which agrees with Southworth's Eq. (11).

In deriving the equation, each source was considered concentrated at a point. Since each element is a vertical wire, an additional factor $\sin\theta$ must be introduced, and if $nNNE_0$ is used as a common voltage level, the equation for the polar diagram becomes:

$$\begin{aligned}r = &\frac{\sin n\pi(a\cos\phi\sin\theta+b)}{n\sin\pi(a\cos\phi\sin\theta+b)}\\&\cdot\frac{\sin N\pi(A\sin\phi\sin\theta+B)}{N\sin\pi(A\sin\phi\sin\theta+B)}\\&\cdot\frac{\sin N\pi(A\cos\theta+B)}{N\sin\pi(A\cos\theta+B)}\cdot\sin\theta. \quad (7)\end{aligned}$$

This equation, which corresponds to Southworth's Eq. (12), includes all possible combinations of equispaced and equiphased arrays in the x, y, z directions. Special cases of the above equation play an important part in antenna design and are treated more fully in engineering papers on the subject.

Electron Microscopic Determination of Surface Elevations and Orientations

R. D. HEIDENREICH AND L. A. MATHESON
The Dow Chemical Company, Midland, Michigan
(Received December 9, 1943)

The methods of determining object thickness in electron microscopy are briefly reviewed. Uncertainties in interpretation of surface replicas from a consideration of intensities alone are discussed and three different replicas of etch figures in pure aluminum are presented. The stereoscopic method is analyzed and an equation is derived relating the parallax of image points in stereo micrographs to the elevations in an object. This equation is the parallax equation of aerial photography but written in the form

$$f=(\csc\sigma/2M)\times 10^3 \text{ microns/mm},$$

where σ is the stereo angle and M the total magnification. The equation is experimentally verified utilizing the cubic etch figures of aluminum. Elevations in the range 0.1–2μ can be determined to within 10 percent and frequently with greater accuracy. A new cartridge for obtaining stereo micrographs at an angle of 10° is described and thicknesses as small as 150±50A are measured using this cartridge. Examples of the use of stereo micrographs are given illustrating different orientations of pearlite in steel and the scratches on a polished steel surface. Elevation changes of 200A and less can be measured in the silica replica of the polished surface. The theoretical resolution of the stereo method is given by

$$x_{\min}=\omega/2\sin\sigma,$$

where ω is the resolution normal to the optic axis and σ is the stereo angle.

INTRODUCTION

THE determination of the spacial arrangements and sizes of structures serving as electron microscope specimens has been, for the most part, confined to two-dimensional measurements in the plane normal to the optic axis of the instrument. As more work is done and experience gained in interpreting the plane photographs, increasing attention is turned toward extending the measurements to the third spacial dimension since the amount of information that can be gained through studying a single projection of an object in space is necessarily limited.

There are at present three distinct ways[1] of estimating vertical distance in electron micrographs none of which applies generally to all electron microscope specimens. Briefly these methods are: (1) Intensities—This method involves the calculation of object thicknesses from photographic plate densities.[1] A somewhat detailed knowledge of the specimen is required, such as atomic scattering cross sections, type of binding, etc. The contribution of inelastic scattering is relatively uncertain in these calculations as is the question as to whether single or multiple scattering applies. There are other complicating factors not taken into account which cannot be readily predicted. Chief among these are the interesting reflections observed in crystalline materials.[2–5] In the case of amorphous materials the computations may be further in error depending upon electrical effects due to accumulation of charges by the material while exposed to the electron beam. The method is thus open to difficulties that must be resolved by further work. (2) Random orientations—The determination of thickness by means of observing a random orientation of objects is quite common in the case of dispersed particles, such as pigments, etc., but is not universally applicable to replica films. The measurements are not limited by object thickness, however, and the technique is suitable where average values over a large number of individuals are required. (3) Stereoscopy—The use of stereo micrographs wherein two pictures of an object are taken at different angles and then viewed with an appropriate device has been described numerous times.[6–11] The electron microscope is

[1] L. Marton and L. I. Schiff, J. App. Phys. **12**, 759 (1941).

[2] B. v. Borries and E. Ruska, Naturwiss. **28**, 366 (1940).
[3] J. Hillier and R. F. Baker, Phys. Rev. **61**, 722 (1942).
[4] R. D. Heidenreich, Phys. Rev. **62**, 291 (1942).
[5] E. Kinder, Naturwiss. **31**, 149 (1943).
[6] W. Eitel and E. Gotthard, Naturwiss. **28**, 367 (1940).
[7] H. O. Müller, Kolloid Zeits. **99**, 6 (1942).
[8] H. Mahl, Zeits. f. tech. Physik **22**, 33 (1941).
[9] M. v. Ardenne, *Elektronen Übermikroskopie* (Julius Springer, Berlin, 1940), pp. 281–286.
[10] R. D. Heidenreich, J. App. Phys. **14**, 312 (1943).
[11] T. F. Anderson, *Advances in Colloid Science* (Interscience Publishers, New York, 1942), Vol. 1, pp. 361–362.

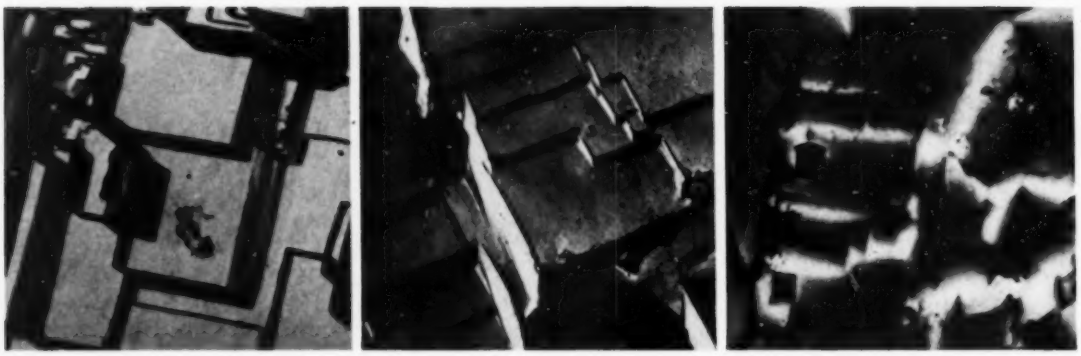

(a) (b) (c)

FIG. 1. Replicas of etch figures in pure Al, 6200×. (a) Anodic oxide film; (b) polystyrene-silica; (c) Formvar.

exceptionally well adapted to stereo work because of its relatively great focal depth. The application is limited by specimen thickness since in order to apply it quantitatively the transmitted intensity must be detected in the photograph; that is, the object must be "illuminated" on both surfaces and also there must be perceptible intensity variations in the image of the surfaces for the eye to focus on.

In the study of surface replicas[8,10] and of particles,[9] the stereo technique is very effective and seems at present superior to all other methods. The use of intensity variations alone in the image of a replica film can be very uncertain and even misleading.[10] This uncertainty is demonstrated in Fig. 1 for three different replica techniques. Figure 1(a) is an anodic oxide film replica[8] of etched, pure aluminum. This replica is likely of uniform thickness over the various orientations of the crystal facets and contrast is obtained in it through the variations in effective thickness as determined by the orientations. Mahl[8] has suggested the determination of the orientations by photographic plate density measurements which yield approximate values for surfaces not steeply oriented to the electron beam but would not easily give information regarding the actual elevations. Figure 1(b) is a silica replica[10,12] of similar etch figures and for this large structure is quite comparable to the oxide films although more distortion has been observed if the films are not handled very cautiously. Finally, Fig. 1(c) is a Formvar replica[13,14] of the aluminum etch structure illustrating the tendency of the plastic lacquer film to fill in the hollows. The upper surface here is far from being level, however, and such a view holds only approximately for elevation changes of the order of the average film thickness or less. From Fig. 1(c) it is estimated that the corners of the rectangular pits are filled in to a depth of about 800A and even then not uniformly but with continuously varying thickness as evidenced by the rounded appearance of the sharp corners. The production of the contrast in the plastic lacquer replicas is described by Gölz.[15] Figure 1, page 9, of his paper exhibits a profile of such a replica which is in agreement with the conclusions from Fig. 1(c). The cubic etch structure in aluminum thus makes an enlightening surface on which to test the replicas.

From each of the replicas of Fig. 1 a general idea of the surface elevations is obtained by visual observation, but in all cases this effect is due to the three-dimensional illusion rather than a consideration of intensities alone. The elevations of these structures can be easily obtained to within 10 percent and the orientations to within five or six degrees at least by the quantitative stereo method as will be described.

THEORY AND PRACTICE OF THE STEREO METHOD

The technique of producing electron stereo micrographs has been discussed before[6,7,9] and

[12] R. D. Heidenreich and V. G. Peck, J. App. Phys. **14**, 23 (1943).

[13] V. J. Schaefer and D. Harker, J. App. Phys. **13**, 427 (1942).
[14] V. J. Schaefer, Phys. Rev. **62**, 495 (1942).
[15] E. Gölz, Zeits. f. tech. Physik **24**, 8 (1943).

will not be considered in any detail here. Suffice it to say that the end result can be obtained either by tilting the specimen with respect to the fixed optic axis or tilting the optic axis relative to the fixed specimen. The present practice is to tilt the specimen plane relative to the optic axis of the microscope with a suitable specimen holder or cartridge. Such a cartridge is available commercially for the RCA type B electron microscope as used in this study* although modified versions can be constructed as will be described.

The viewing of the stereo micrographs is of chief concern here. Devices for viewing and making precision measurements of elevations have been developed for aerial mapping and surveying[16] and are well adapted to electron stereo micrographs since the chief difference is one of order of magnitude of the dimensions involved. One instrument which has proven satisfactory for this work is the Abrams Contour Finder.** This device measures directly the parallax between image points of the individual photographs of a stereo pair after which the parallax readings must be converted to elevations. The conversion of parallax measurements to actual elevations will next be considered in some detail.

The relation between the parallax and surface elevation† can be determined either by calculation or by direct calibration against a surface possessing known elevation changes. The latter is unsatisfactory due to difficulties in obtaining sufficient transmitted intensity through solid particles large enough to be a reliable standard. The calculation of elevations is done through the aid of Fig. 2, wherein the specimen is considered to be fixed and the optic axis tilted through the total stereo angle 2σ. This construction is equivalent to tilting the specimen through an angle $\pm\sigma$ to either side of the horizontal. A represents an elevation on the specimen plane of height x. For simplicity, point C is chosen such that the projections of A and C (A_2 and C_2) coincide in the right-hand image. In the left-hand image they are separated by the distance $y=A_1C_{1N}$, the parallax of the points A and C in the stereo micrographs. If M denotes the final magnification of the image, then

$$y=AB_{N}M$$

and to good approximation

$$AB_{N}=2x\sin\sigma$$

so that the parallax is given for small δ by

$$y=2Mx\sin\sigma.$$

Differentiating with respect to y yields the rate of change of elevation with respect to parallax or the conversion factor f,

$$f=dx/dy=\csc\sigma/2M. \qquad (1)$$

In aerial photography, (1) is termed the parallax equation and is expressed in terms of the altitude from which the pictures are taken, the distance between pictures and the focal length of the camera. Parallax measurements are simply multiplied by the value of f from Eq. (1) to convert

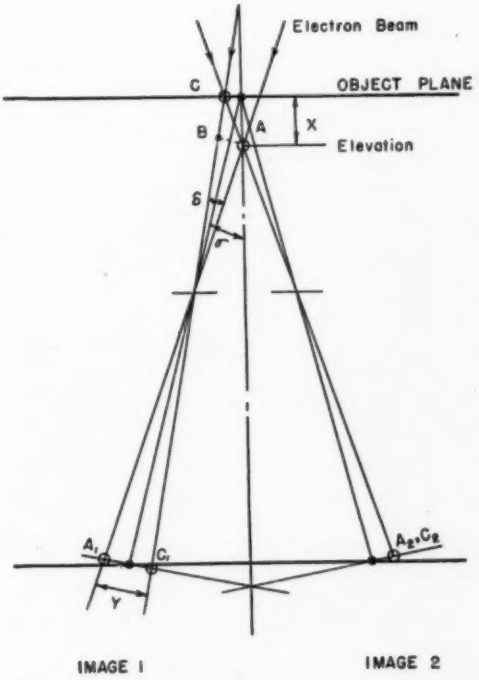

FIG. 2. Parallax construction for stereo images.

* RCA Manufacturing Company, Camden, New Jersey.

[16] J. W. Bagley, *Aerophotography and Aerosurveying* (McGraw-Hill Book Company, Inc., New York, 1941), Chapters 9, 11, and 12.

** Full details can be obtained from Abrams Instrument Company, Lansing, Michigan.

† Since this was written, reference to similar calculations has come to notice, but no details were available at the time. See Chem. Abstracts **36**, 6173 (1943).

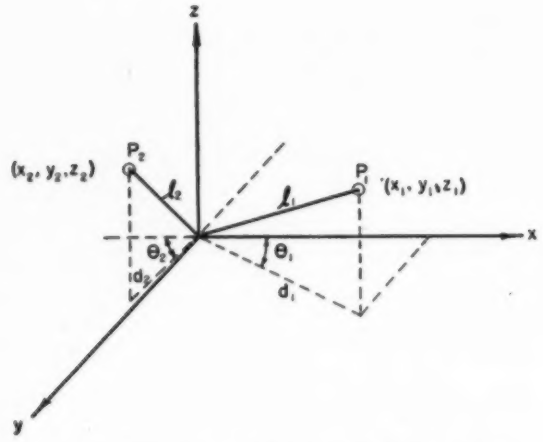

FIG. 3. Geometry of intersecting edges in cubic etch structure.

them to elevations. It is convenient to express f in microns per mm of parallax for this work, so that (1) is written

$$f=(\csc\sigma/2M)\times 10^3 \text{ microns per mm.} \quad (2)$$

One way of testing Eq. (2) is by means of a replica of the cubic etch structure of aluminum, such as Fig. 1(a). The only fact that need be known for this purpose is that the structure is actually rectangular. This is the case here since the exposed facets are {001} planes of the metal.[8] To use this structure for calibration, in Fig. 3 let OP_1 and OP_2 be any two intersecting edges in the etch structure and denote by θ_1 and θ_2 the projections of the direction angles with the x axis on the x–y plane. Denote the direction angles of OP_1 and OP_2 as α_1, β_1, γ_1 and α_2, β_2, γ_2, respectively, and noting that OP_1 and OP_2 intersect at right angles, there obtains

$$\begin{aligned}\text{Cos }\alpha_1\text{ Cos }\alpha_2+\text{Cos }\beta_1\text{ Cos }\beta_2\\ +\text{Cos }\gamma_1\text{ Cos }\gamma_2=0.\end{aligned} \quad (3)$$

Further, it is seen from the figure that

$$\begin{aligned}&\text{Cos }\alpha_1=\text{Cos }\theta_1\text{ Sin }\gamma_1;\\ &\text{Cos }\alpha_2=-\text{Cos }\theta_2\text{ Sin }\gamma_2;\\ &\text{Cos }\beta_1=\text{Sin }\theta_1\text{ Sin, }\gamma_1;\\ &\text{Cos }\beta_2=\text{Sin }\theta_2\text{ Sin }\gamma_2.\end{aligned} \quad (4)$$

By (3) and (4)

$$\begin{aligned}\text{Cot }\gamma_1\text{ Cot }\gamma_2&=\text{Cos }\theta_1\text{ Cos }\theta_2-\text{Sin }\theta_1\text{ Sin }\theta_2\\ &=\text{Cos }(\theta_1+\theta_2).\end{aligned} \quad (5)$$

Now let the parallax readings, relative to the origin, with the x axis taken as the "stereoscopic base," be y_1 and y_2, so that

$$z_1=fy_1$$

and

$$z_2=fy_2,$$

where f is the conversion factor as before. Since $z_1/d_1=\text{Cot }\gamma_1$, Eq. (5) finally becomes

$$f^2=(d_1d_2/y_1y_2)\text{ Cos }(\theta_2+\theta_1). \quad (6)$$

Equation (6) can be employed to check the con-

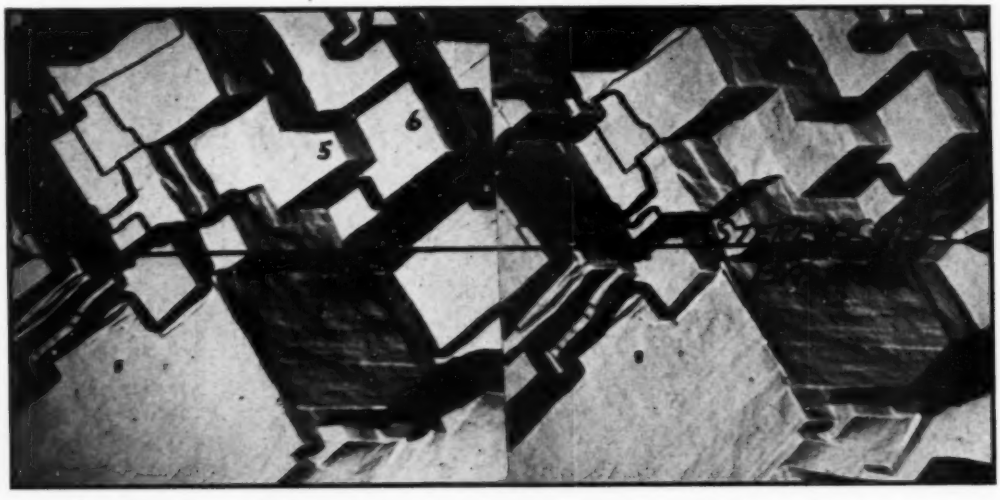

FIG. 4. Stereo electron micrograph of cubic etch structure in pure aluminum aligned for calibration of contour finder, 5600×.

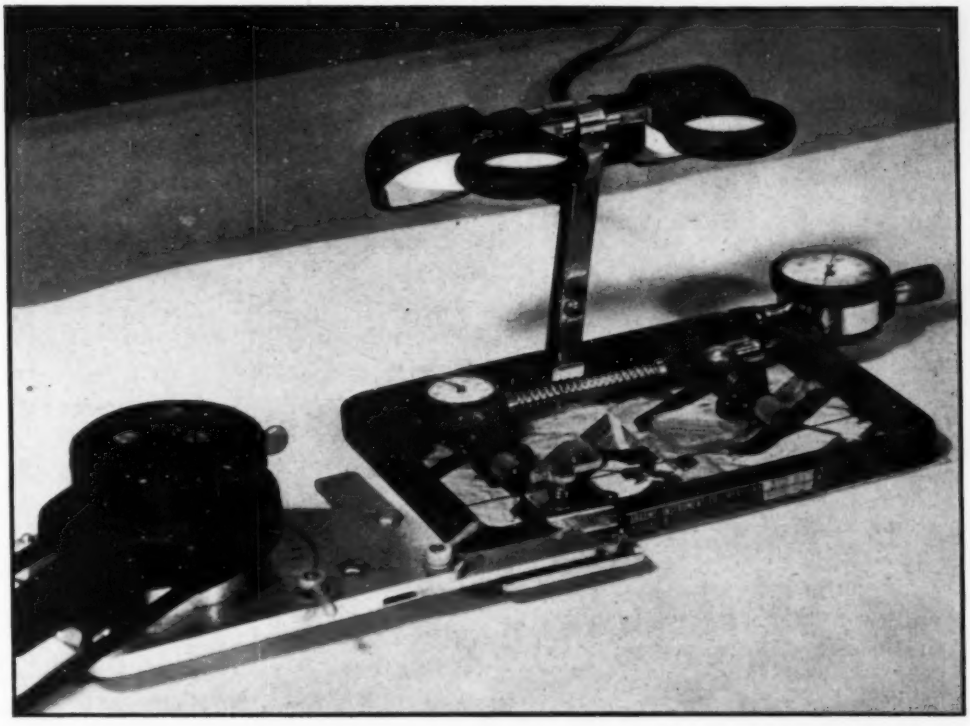

FIG. 5. Contour finder set up over electron stereo micrographs for parallax measurements.

tour finder since all quantities on the right side can be determined directly from the photographs. The angles θ_1 and θ_2, as well as the projected lengths d_1 and d_2, are measured on both photographs of the stereo pair and the average values used in (6). The arithmetical averages are sufficiently exact for this purpose.

The "stereoscopic base" mentioned above is the intersection of the plane in which the angle $\pm\sigma$ is turned with the plane of the photographs (i.e., perpendicular to the axis of rotation) and must be determined independently. This can be done by mounting a small fiber in the stereo cartridge, carefully aligning it in the plane in which the stereo angle is to be realized, and then photographing it in the microscope. This must be done for the several settings of the projector lens current since the magnetic lenses rotate the image about the optic axis. The image of the fiber thus obtained will then serve as the stereoscopic base line for aligning the stereo micrographs taken subsequently. The accuracy of the base line location as so determined is sufficient since the calibration is insensitive to small deviations in the base line. A short calculation shows that an error of 5° in the setting of the base line will make only a 0.4 percent error in the conversion factor to be used, while a 20° error changes it by only about 5 percent. If the stereoscopic base line is determined to within 10°, the error will be less than others arising in the technique.

The plate with the images of the fiber serving as the stereoscopic base calibration is employed as a standard for indexing all subsequent micrographs. One procedure for preparing the prints for parallax measurements is as follows: (1) Index the negative from the standard base line calibration plate and print. Draw lines through the index marks on the prints to serve as the stereoscopic base. The base line is usually drawn through the print centers. (2) Mount one print securely on a drawing board with the wandering dots of the contour finder set on the stereoscopic base. The instrument should be affixed to a drafting arm to maintain alignment for all subsequent measurements. (3) While viewing through the stereoscope, adjust the other print so that the two images fuse. The base lines of both prints should be parallel if

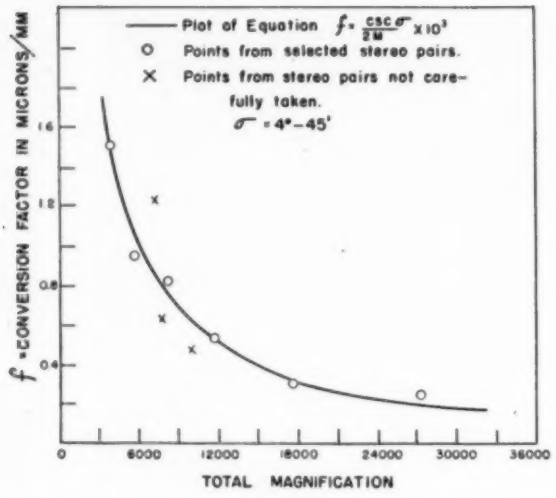

FIG. 6. Experimental verification of parallax equation.

the micrographs were taken accurately. Securely fasten both prints to the board and measure the parallax between the chosen image points.

Figure 4 shows a pair of electron stereo micrographs with the base line marked and aligned for carrying out the measurements. This structure is an anodic film replica[8] of pure, as-cast aluminum etched 20 minutes in 1 : 1 hydrochloric acid-methanol. The anodic film was produced in a distilled water solution containing 2.5 percent ammonium borate and 0.2 percent boric acid at 20 volts for about 2 minutes. Figure 5 is a photograph of the contour finder set up over a pair of electron stereo micrographs.

Some observations concerning the alignment of the prints are as follows: (1) The measurements are independent of whether the final magnification is obtained photographically or in the microscope. The final magnification should be such that the parallax to be measured falls within the range of the contour finder. (2) Changing the separation of the prints while maintaining the base line alignment does not affect the relative parallax readings. Inverting or interchanging the prints results only in changing the sign of the reading. There is usually one arrangement that is superior as far as viewing is concerned which can be determined by trial.

Measurements from stereo pairs such as Fig. 4, aligned as just described, were employed in Eq. (6) to check Eq. (2). Each point consists of measuring for any two intersecting edges the angles θ_1 and θ_2, the projected lengths d_1 and d_2, and the parallax relative to the intersection. θ_1 and θ_2 should be measured from the base line for calibration purposes. Several likely looking corners in each stereo pair were employed to obtain an average value. Corners which were obviously distorted were avoided. Figure 6 shows a plot of Eq. (2) for the RCA cartridge and some experimental points determined as just described. The crosses are data from stereo pairs taken with no special precautions as to adjusting the cartridge. The circles resulted from pairs selected for the purpose of calibration on the basis of the accuracy with which the cartridge was set between pictures.

WIDE ANGLE STEREO CARTRIDGE

The accuracy and resolution of the contour finder increase with both stereo angle and magnification. In order to extend the range of measurements a new cartridge was constructed which allowed an angle of $\sigma = 10°$ to be realized as well as higher magnification. The latter is produced by increasing the length of the cartridge.[17] This is not possible with the RCA type cartridge, but when constructed as shown in Fig. 7 cartridges of greater length (17 mm or slightly more) can be utilized. The revolving barrel is eliminated in the design of Fig. 7 and the tilting of the specimen plane is accomplished by rotation of the specimen ring about a pivot. The ring and pivot pins are machined from a single piece of brass with the axis of rotation accurately located in the plane of the specimen so that the same region may be found when the ring is tilted first one way and then the other. Location of the centers of the pivot pins in the specimen plane can be accomplished by drilling a small hole (No. 76 drill) through the ring and pins to serve as an axis or center line. The shoulder in the ring serving as the specimen plane is then cut so that it bisects the fine hole drilled through pins and ring. The hole through which the electron beam enters the specimen must be accurately centered so as not to shade out a portion of the field when the ring is tilted. The construction of the ring is

[17] C. J. Burton, R. B. Barnes, and T. G. Rochow, Ind. Eng. Chem. **34**, 1429 (1942).

the most difficult part of the cartridge and must be done carefully if the cartridge is to work properly.

With the present design, the ring cannot accommodate the ordinary specimen screen but only a portion thereof and hence trimming is required. A ring which will take a full diameter screen necessitates a total diameter for the lower end of the cartridge too great to allow sufficient motion of the movable stage without contacting the sides of the objective pole piece. The screen is retained in the ring by means of a disk or plate bearing a small hole or limiting aperture. This limiting aperture was found necessary in order to confine the stereo fields to the central region of the ring. Pictures taken at the two settings with angles as great as $\pm 10°$ will exhibit a considerable magnification discrepancy if they are not confined to the region of the axis of tilt. The effect of such a magnification discrepancy will be discussed in the next section. This precaution is not so necessary with the RCA cartridge using the smaller stereo angle, but pictures from the central region of the specimen screen yield more accurate results.

The retaining disk is held firmly in the ring, against the specimen screen, by means of a beveled cap which simultaneously presses the ring against the shoulder of the cartridge barrel and maintains the stereo angle. The first micrograph is taken with the cap in one position after which the cartridge must be removed from the microscope and the cap removed and replaced again but turned 180° from the initial position. Turning of the barrel or reversal of the cartridge between pictures is not required with the result that possible variations in settings from one stereo pair to another are considerably less.

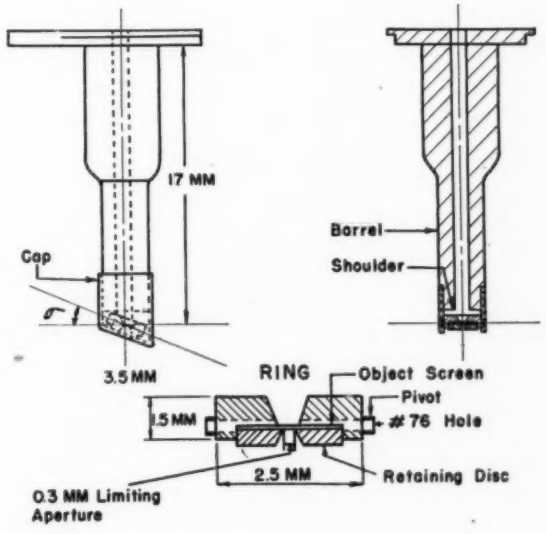

FIG. 7. Detail of wide angle stereo cartridge.

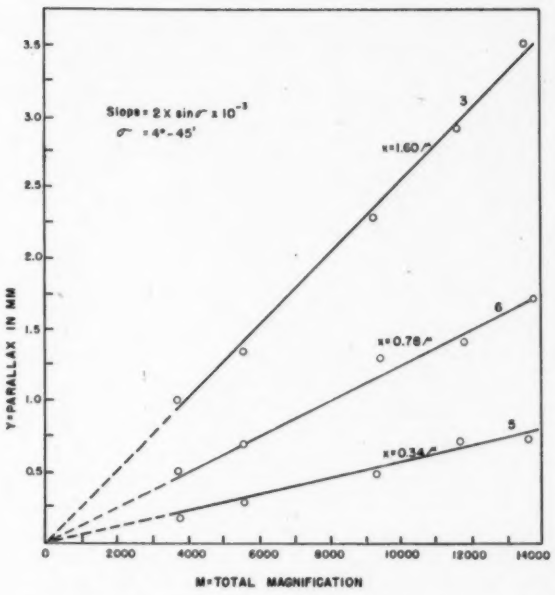

FIG. 8. Parallax—magnification plots for checking cartridge and readings, and for computing elevations. The lines correspond to edges 3, 5, and 6 of Fig. 4.

Any desired stereo angle can be incorporated into the cartridge by filing either the shoulder of the barrel or the edges of the ring. The angle of $\pm 10°$ was chosen in this case in order to extend the range of vertical measurements down to 100–200A and still maintain a reasonable accuracy without resorting to excessive photographic enlargement.

CARTRIDGE CALIBRATION

The cartridge can be calibrated as previously described using the aluminum etch figures, but a more convenient manner of checking the accuracy of any cartridge is to be desired. The measurements from the aluminum etch figures utilizing Eq. (6) constitute an external or absolute calibration and can be considered to be sufficient to establish experimentally the applicability of Eq (2).

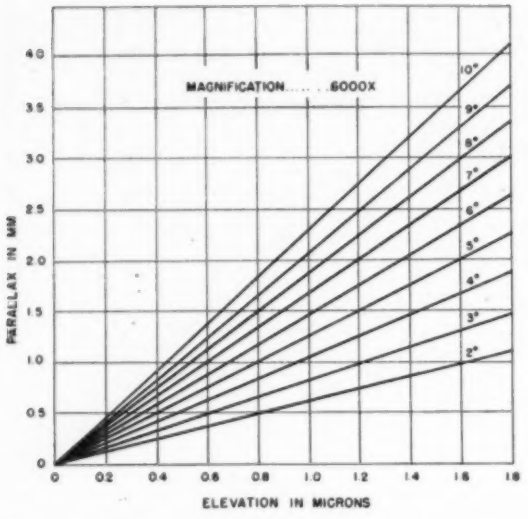

FIG. 9. Standard chart for checking parallax readings and elevations for various stereo angles. A magnification of 6000× was chosen for this plot, but charts can be prepared for any magnification.

A convenient method of checking the magnification dependency of Eq. (2) for any stereo pair is to plot the parallax readings for several points obtained from a series of enlargements against the total magnification as in Fig. 8. A straight line will be obtained for each elevation, which extrapolates through the origin if Eq. (2) is strictly obeyed. The slope of the family of such lines is given by $2x \sin \sigma \times 10^{-3}$, so that knowing σ the elevations can be easily computed from the slopes. Should it come about that the data do not yield straight lines passing through the origin, then the parallax equation is not directly applicable and the conclusion is that the stereo micrographs exhibit a magnification error or are not sharp and either must be corrected or discarded.

The lines of Fig. 8 correspond to edges 3, 5, and 6 of Fig. 4 and it follows from slope measurements that the elevations corresponding to these edges are 1.60μ, 0.34μ, and 0.78μ, respectively. It is recommended that in all work where any precision is desired plots similar to Fig. 8 be prepared and the elevations determined in this way.

ACCURACY AND RESOLUTION

There are several factors to be considered in the evaluation of the accuracy of the stereo technique. To begin with, high quality micrographs and prints are necessary since photographs that are not sharp and clear have been found to be unreliable for quantitative measurements. Such images do not furnish sufficient common structure in the two pictures to focus on while viewing.

One source of error is the stereo angle σ. σ can be determined by either optical or mechanical methods and should be known within an accuracy of 5 percent or better Another error is lumped into the removal and insertion of the cartridge into the microscope, printing and making the actual parallax measurements. From stereo pairs taken consecutively and printed and aligned similarly, the reproducibility has been found to be about 5 percent and sometimes better.

The accuracy of elevation determinations will be no better than that of the magnification calibration of the microscope. Techniques of calibration have been described[17] which make a precision calibration of magnification relatively easy to obtain.

The actual parallax measurements as made with the contour finder require practice, but a skilled operator should be able to reproduce measurements consistently to within 0.02 mm on a specimen exhibiting distinct elevation changes. Several readings should be taken both "up" and "down" on the image points in question. In order to realize an accuracy of 5 percent in the parallax determinations if the uncertainty is 0.02 mm, it is necessary that the stereo angle or magnification be such that the parallax of the two image points is 0.4 mm or greater. As previously stated, plots such as Fig. 8 should be employed for precision work with more than one stereo pair used to produce the enlargements. The maximum photographic enlargement that can be employed depends upon the quality of the micrographs and the structure being measured. Enlargements of 6–8× can be employed which give a total viewing magnification of 24–32× since the oculars of the contour finder magnify 4×.

It is desirable to check the cartridge and contour finder from time to time and, if precision work is being done, checks should be made for each pair taken. This can be quickly accomplished by preparing a plot similar to Fig. 8, measuring the slopes and computing the eleva-

tions and then checking the elevation so determined against a standard chart such as is shown in Fig. 9. This chart was prepared taking 6000× as a standard magnification, but a similar one can be computed for any magnification. Any stereo pair of a total magnification of 6000× taken at a stereo angle of 2°–10° can be checked against Fig. 9.

The final source of error to be mentioned is that arising from a magnification discrepancy between the individuals of a stereo pair. Such a discrepancy makes itself apparent through difficulty in aligning and stereoscopic focusing and always results in what is termed "tilt" in aerial photographs in addition to altering the parallax along the stereoscopic base. This is equivalent to introducing parallax in a direction different from that produced by the stereo angle. Tilt can be measured with the contour finder by means of the micrometer attached for this purpose, but it is desirable to eliminate such a correction by obtaining both micrographs at the same magnification. If the discrepancy exceeds about 6 percent the correction is usually too great to be measured for elevations of the order 0.4μ or greater. The safest method is to eliminate the necessity for correction by taking all stereos near the center of the cartridge. This is the purpose of the limiting aperture in the retaining disk of the 10° cartridge shown in Fig. 7. Smaller magnification discrepancies will also be made known through poor reproducibility and tendency for the points to scatter considerably in plots such as Fig. 8. The diameter of the limiting aperture that can be used in a cartridge such as Fig. 7 in order that the magnification discrepancy be not more than 1 percent is given by

$$d = 0.08 \text{ Cot } \sigma \text{ mm.} \qquad (7)$$

Thus, $d = 0.4$ mm for $\sigma = 10°$ and $d = 1$ mm for $\sigma = 4°$.

The question of resolution invariably arises in all phases of electron microscopy and stereoscopy is no exception. The stereo technique alone places no limitation on the dimensions of the smallest elevation changes that can be measured, for by increasing the stereo angle and/or magnification, the conversion factor of Eq. (2) can be made as small as desired. The limitation is dictated by the quality of image produced by the microscope and

FIG. 10. Electron micrograph of kaolin clay crystals from stereo pair taken with stereo angle of ±10°. Thickness of crystal No. 1 as measured with contour finder is 140±50A.

it is the resolution of the instrument that fixes the resolution of the stereoscopic measurements. Elevation changes or thicknesses of the order 150–700A can be readily measured with the contour finder when a stereo angle of 10° is employed and high quality images are produced. Figure 10 shows one micrograph from a pair taken of kaolin clay crystals supported on a silica substrate. Determination of the thickness of the crystal marked "1" yielded a value of 140A with an uncertainty of ±0.01 mm of parallax corresponding to ±8A on the scale of the photograph. The actual uncertainty is considered to be the vertical resolution of the microscope so that a value of perhaps ±50A is taken as the probable error in the determination. Measurements of other crystals from the same plate as Fig. 10 gave values of 150A and 160A with an average thickness for these crystals of 150±50A.

An approximate calculation of the vertical resolution or smallest thickness that can be measured stereoscopically is of interest. If ω denotes the minimum lateral discontinuity in structure of the object that can be detected, then from Fig. 2 or Eq. (2) the minimum elevation or thickness change that can be measured is

$$x_{\min} = \omega/2 \text{ Sin } \sigma. \qquad (8)$$

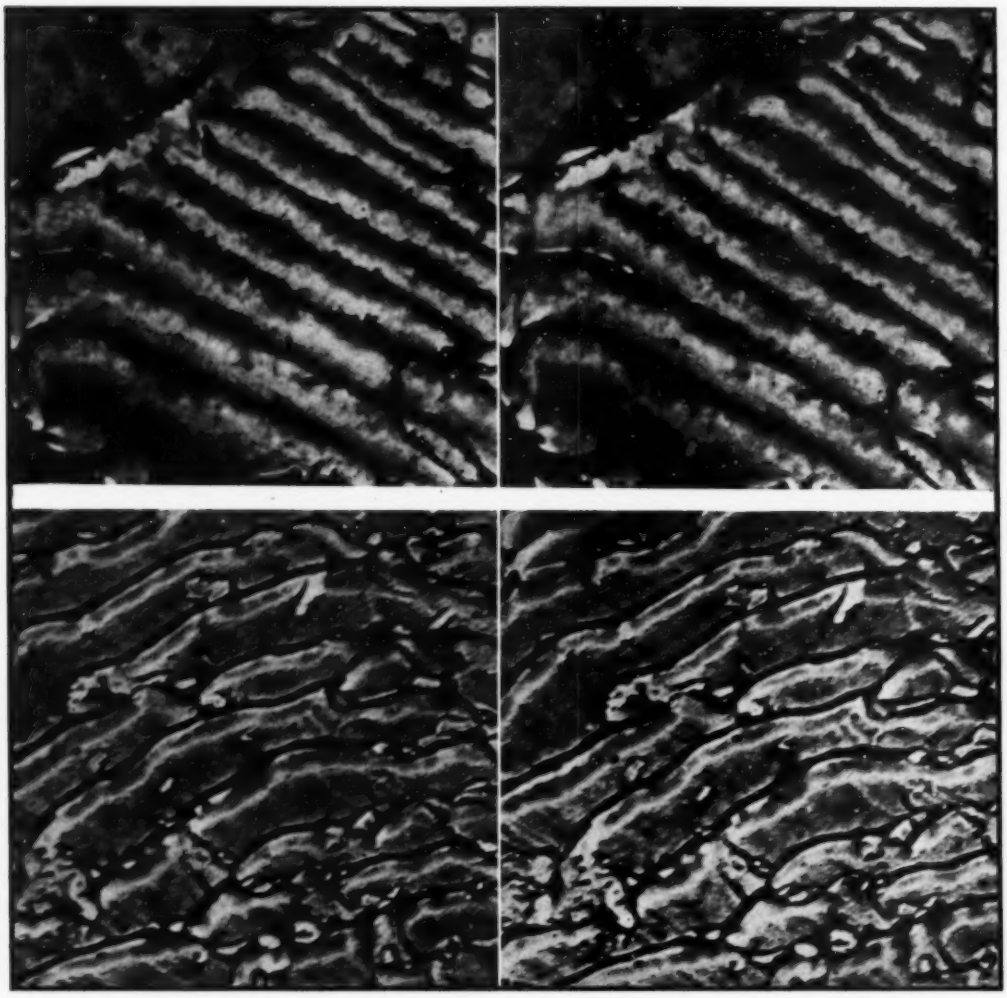

FIG. 11. Lamellar pearlite in 0.50C steel, 12000×; $\sigma = 4° 45'$. (a) Lamellae nearly normal to surface; (b) lamellae oblique to surface.

For $\omega = 35$A and $\sigma = 10°$, the vertical resolution x_{min} would be about 100A. This value is uncertain depending upon the value of ω, but it is apparently of the right order in view of the measurements from Fig. 10. The vertical resolution as given by Eq. (8) is also, of course, a measure of the minimum uncertainty in a vertical measurement as well as of the minimum distance which can be detected. The values from Fig. 10 are slightly less than the resolution given by Eitel and Gotthard[6] of 200±50A, but the stereo angle is probably greater than that employed by them. On the basis of the above calculation a stereo angle of 20° would be required in order to measure thicknesses of 50A, but until more work is done concerning resolution and its measurement in electron microscopy these calculations must be considered only rough approximations. Meanwhile, it may prove possible to extend stereoscopic measurements down to 100A by careful work in producing suitable images. Phenomona such as diffraction at the edges of discontinuities where measurements are generally made are to be considered, but just what their effect will be has not been investigated.

EXAMPLES

The technique of quantitative stereoscopy described in the preceeding sections obviously has a multitude of applications not only in surface

replica work but in particles, pigments, etc., as well. The method of calibration of the contour finder suggests immediately the determination of the orientation of the crystals in metals. Thus if the stereoscopic base is taken as the x axis and the x–y plane as the polished aluminum surface, the direction angles of a normal to a {001} plane of Fig. 4 are found from Eqs. (4) to be $\alpha=72°$, $\beta=59°$, and $\gamma=36°$. This could be extended to the determination of face pole figures in fine grain aluminum by taking numerous stereo pairs and determining the orientation with the contour finder. Although the anodic oxide film is unique to aluminum containing not more than a few percent alloying constituents, the silica replica can be used for this purpose on any metal in which it is possible to obtain a crystallographic etch attack.

In addition to the determination of crystal orientations in a pure metal the measurement of orientations and elevations of precipitated phases in alloy systems is of importance. An example of two different orientations of the same type of structure is shown in Fig. 11, (a) and (b). These are stereo micrographs of polystyrene-silica replicas of lamellar pearlite in a 0.50C steel electrolytically polished and then etched in picric acid-ethanol. Figure 11(a) exhibits the lamellae oriented nearly normal to the surface with an average spacing of about 0.6μ, an average height of 0.15μ, and a thickness of 0.1μ. In Fig. 11(b) the lamellae are inclined to the surface at an average angle of roughly 20° covering a range of from 10° to 40°. They project about 0.15μ out from the ferrite with a spacing of approximately 0.5μ as determined stereoscopically. A rough measurement of the spacing from a single print as obtained by simply placing a scale across it gives a value of 0.8–1.0μ illustrating the importance of determining orientations in measuring any quantities concerning surface structures.

It is possible that in measurements of the spacings of glide lamellae,[18] mosaic structures, etc., the results may be in considerable error if the structures are obliquely oriented to the surface and are not so treated. Again a qualitative stereoscopic observation of such structures will often make their contours immediately evident and eliminate the speculation that otherwise will result. The question as to which is the correct viewing arrangement and whether the elevations should be depressions or vice versa cannot always be determined from the stereo micrographs alone, but in many cases auxiliary information will make only one arrangement logical. In other cases, the question of up and down can usually be settled by simply studying the stereo micrographs with special attention to near-vertical sides on what might be step structures, etc. Structures of the type of Fig. 1 often exhibit dark corners or edges in the silica replicas due to the tendency of silica to accumulate in sharp discontinuities.[10] From the present viewpoint these darker edges, such as in Fig. 1(b), should appear high in the stereoscope and so may serve as an index for determining whether the structure should be up or down.

Although many illustrations of the application of stereo micrographs could be given only one more will be considered here. Figure 12 is from a stereo pair taken of a silica replica of a polished steel surface. The final finish was obtained on a felt wheel using MgO abrasive in water. Some coarser grits of Al_2O_3 were present on the wheel which left larger scratches on the polished surface such as the one on the right-hand side of Fig 12.

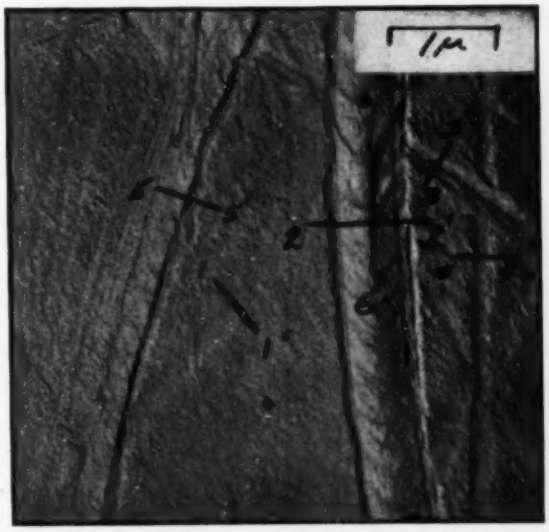

FIG. 12. Electron micrograph (polystyrene-silica replica) showing scratches in a polished steel surface. The lines drawn in are those along which the profiles of Fig. 13 were measured.

[18] C. S. Barrett, Metals Tech. **10** (Sept. 1943).

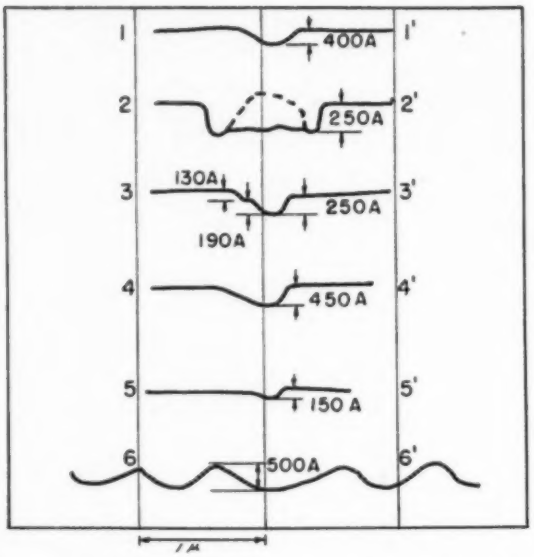

FIG. 13. Profiles of the scratches indicated in Fig. 12 as measured with the contour finder.

The stereo pair was taken with the cartridge shown in Fig. 7 and a stereo angle of 10°. Profiles of several scratches were determined with the contour finder along the sections marked on Fig. 12 and are shown in Fig. 13. The contours are on quite a small scale but show up quite strikingly as can be seen stereoscopically in the enlargements of Fig. 14.

The wide groove is of interest due to its peculiar shape and structure and gives rise to speculation as to just how it might have come about. There seems to be a periodic structure along the length of the track having an average periodicity of about 0.4μ. The appearance would suggest that the particle that caused this scratch was concave in the region that contacted the metal as might result from two sharp projections on the particle about 0.7μ apart. Inasmuch as the deep edges do not show the periodic structure found in the center, it is suggested that this structure came about through melting at the "bow" of the particle followed by freezing again at the "stern" with the shape resulting from the tendency of the molten metal to be pushed toward the center. Another possible explanation is that the particle "chattered" as it cut through the metal. From the speed of the wheel, a frequency of 10^5–10^6 cycles per second would be necessary to give the periodicity observed. If this were the case, however, the deep edges of the groove would be expected to exhibit the same periodicity so that the evidence would be in favor of the melting theory. This observation suggests many interesting experiments that might be performed in studies of grinding and polishing.

CONCLUSION

The stereoscopic technique has proven satisfactory for quantitative determination of elevation changes over the range 0.015–3μ. The upper

FIG. 14. Enlargement of stereo pair from region of Fig. 12 illustrating appearance of wide groove and various scratches.

limit of measurements is set only by the depth of focus of the electron microscope with the lower limit dependent upon the resolution of the instrument. Elevations exceeding 3μ have only rarely been encountered in replica applications.

The method can be applied to a great variety of electron microscope specimens but is restricted to thicknesses which give a detectable transmitted intensity. Qualitative observations on objects of too great a thickness to allow sufficient transmitted intensity for actual measurements are frequently useful for gaining an idea as to clustering, orientation, etc.

The indications are that surface replicas will offer the greatest field for application of the technique. A misconception concerning the interpretation of surface replicas, both silica and Formvar, seems to have arisen which often leads to erroneous conclusions about the contours of the original surface. Figure 1 is intended to demonstrate the error in assuming that the upper surface of these replicas is flat. The silica tends to accumulate in sharp elevation changes but on a scale less than that of the Formvar films and for large structures should be interpreted in a manner similar to that of the aluminum oxide films.[8,10] The Formvar likewise should be viewed as not possessing a level upper surface but rather as following the surface contours in a rounded fashion such as to give thickness variations that are not abrupt. It is this departure from a level upper surface in all cases that makes interpretation of the electron micrographs more complex when intensity variations alone are considered.

Qualitative stereoscopy will do much to clear up these difficulties and should be freely employed in any surface study if misinterpretations are to be avoided. Quantitative stereoscopy will yield still more information and must be considered necessary to quantitative work on surface structures.

It is worth mentioning that in stereoscopic viewing the eye tends to focus on fine details rather than a blank surface. Consequently, in observing and measuring stereo micrographs of surface replicas, the surface of the replica bearing the structural details is the one that fixes attention. Contours observed in a replica are thus the actual contours of the original surface providing distortion of the replica film has not occurred during handling.

The provision of more convenient and more precise attachments on the electron microscope for the production of stereo micrographs, such as a universal stage allowing tilting of the object to any desired angle by external control, would greatly simplify the stereo technique and eliminate the necessity of building special cartridges.

Rate of Rise of Water in Capillary Tubes

WILLIAM A. RENSE
Louisiana State University, Baton Rouge, Louisiana
(Received January 24, 1944)

SOME results in connection with the rise of water in a capillary tube have been obtained which may prove of some interest to the readers of this journal.

The well-known formula for the ultimate height to which the water will rise has often been verified for clean tubes of uniform bore. But few data have been presented on the nature of the rise itself. Poiseuille's law does not apply here because dv/dt is not zero. Furthermore, because the velocity of the water as it rises changes rapidly (at least over part of the rise), one would expect a resistive force to exist which is not taken into account in the standard equations for viscous flow. Such frictional pressure drops, attributed to turbulence, are observed in many instances of fluid flow, and invariably tend to follow a velocity-squared law. On the assumption that the rise of water in a capillary tube is turbulent, it is easy to explain the character of the rise. The writer has done so, and has verified his results with measurements from stroboscopic photographs.

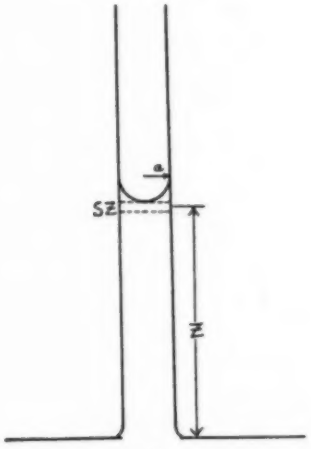

FIG. 1.

When the tube is first inserted there results an impulsive force which causes the top element of water to acquire a very high speed up the tube in an extremely short time. The force results from the fact that the pressure immediately below the meniscus, because of surface tension, is much less than atmospheric pressure which prevails elsewhere at the surface of the surrounding liquid. The impulsive force ceases action as soon as the liquid in the neighborhood of the orifice assumes a motion that adjusts to the pressure differences. The impulsive aspect of the rise is not revealed on the photographs taken for this study, for the time interval used ($\frac{1}{20}$ sec.) was far too great to cover the early motion.

While the water is moving upward after the impulsive pressure ceases, the following expression represents the motion of a thin cylindrical section of length δz and instantaneous speed v:

$$\pi a^2\delta z(dv/dt)=\pi a^2\delta z g+\pi a^2\delta p+\pi a^2\delta p', \qquad (1)$$

where a is the radius of the tube, δp is the pressure difference along the section (due to gravity), and $\delta p'$ is the drop due to friction (Fig. 1). Each thin section of water in the tube is subject to a change in speed which is communicated to it by an adjacent section and which it must in turn communicate to the opposite adjacent section. In a non-compressible ideal fluid the transmission

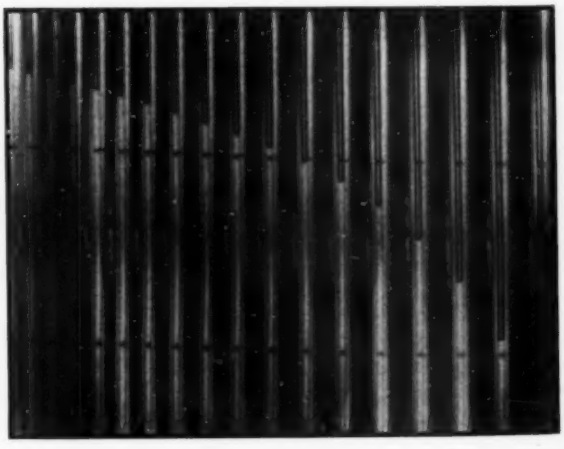

FIG. 2.

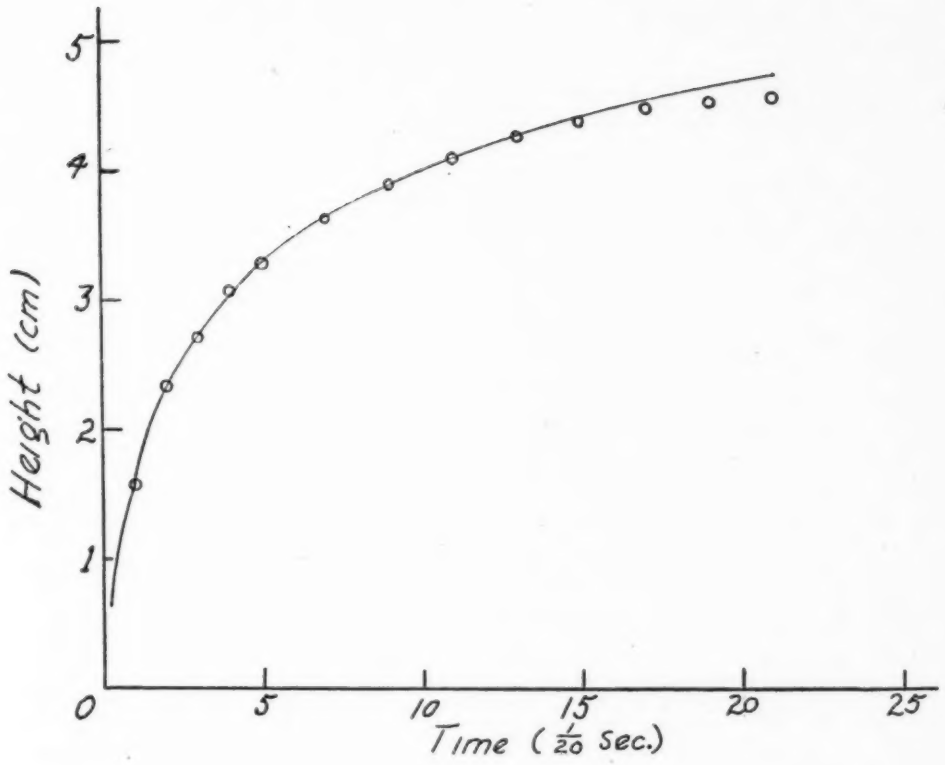

FIG. 3.

occurs instantaneously. But any real fluid has viscosity, and there result a lag and consequently eddies and dissipation of energy in the form of heat. We might, therefore, expect the flow of water to be a turbulent one in the case of capillary rise, and we set:

$$\delta p' = -k^2 \delta z v^2, \tag{2}$$

where k^2 is a constant. Moreover, in (1), δp is merely the increase in pressure due to depth, and equals $-g\delta z$. Substituting in (1) and dividing by πa^2 we get:

$$dv/dt = -k^2 v^2. \tag{3}$$

The first integral of (3) gives:

$$1/v = k^2 t + \text{constant}.$$

We set the constant equal to zero, for when $t \to 0$, $1/v \to 0$, assuming that the impulsive force produced a relatively high velocity. The second integral gives:

$$z = \text{constant} + (1/k^2) \log t. \tag{4}$$

This is the equation for the rise if it is turbulent.

The rise of water in a capillary tube of radius 0.0316 cm was photographed several times in stroboscopic light of interval $\frac{1}{20}$ sec. (see Fig. 2). Measurements were taken of the height z cm at instant t seconds after the rise. The circles in Fig. 3 refer to the observed points. The resulting curve z *vs.* t was found to be best represented by the equation

$$z = 4.65 + 1.04 \log t. \tag{5}$$

This is the curve shown in the figure and agrees very well with the observed data except for points at the end of the rise where a deviation is to be expected because it is just here, at slow speeds and accelerations, that the causes of turbulence would no longer exist. These results therefore suggest a dynamic method for finding Reynolds number.

Mechanical Models of Frequency Converters

HARRY STOCKMAN
Cruft Laboratory, Harvard University, Cambridge, Massachusetts
(Received December 13, 1943)

The action of modern frequency converters can be lucidly and accurately described by easily-built mechanical models, which for a chosen type of operation record the output wave as function of input amplitudes and input frequencies.

FREQUENCY conversion is usually treated as a sort of modulation or demodulation, founded on conventional modulation or detection theory. Although modulation, detection, and frequency conversion are closely related, they are in principle different.[1] Modulation means putting a signal into a wave and demodulation or detection means recovering the signal from the wave. Frequency conversion or frequency changing, however, means shifting the frequency of the wave. The device that performs the shift is known as a frequency changer or frequency converter. The action of such a device may be studied by means of the mechanical models described in the following, which models demonstrate as well the action of fundamental types of modulators (see Fig. 1).

GENERAL CONSIDERATIONS

The general expression for a carrier wave of angular velocity $A=2\pi f_A$, amplitude modulated by a local wave of angular velocity $B=2\pi f_B$, may be written

$$e=E_{A\ \max}(1+m_a\cos Bt)\cos At, \qquad (1)$$

where e = instantaneous voltage of modulated wave,
$E_{A\ \max}$ = amplitude of carrier wave A,
$E_{B\ \max}$ = amplitude of signal wave B,
$m_a=E_{B\ \max}/E_{A\ \max}$ = degree of modulation.

This particular form of the instantaneous voltage e suggests that the major action of a modulating device is to create a product term of the type $\cos At\times\cos Bt$. Physically e has the form of the carrier and side frequencies,

$$e=E_{A\ \max}\cos At+\tfrac{1}{2}m_aE_{A\ \max}\cos(A+B)t+\tfrac{1}{2}m_aE_{A\ \max}\cos(A-B)t. \qquad (2)$$

The time plot of e shows an envelope with sinusoidal pulsations of B frequency, and the shape of this envelope suggests that the wave may be produced by a mixing device, or mixer, of variable admittance, transadmittance, or gain; the admittance, transadmittance, or gain being controlled by the B source. Generally, when the B source increases the mixer gain, the output wave is expanded, and when the B source decreases the mixer gain, the output wave is contracted. The periodic variation of the gain creates the product term, representing the sum and difference frequencies, which together with the carrier wave constitute the modulated output wave.

A modulating device inherently acts as a frequency converter, as it gives rise to new frequen-

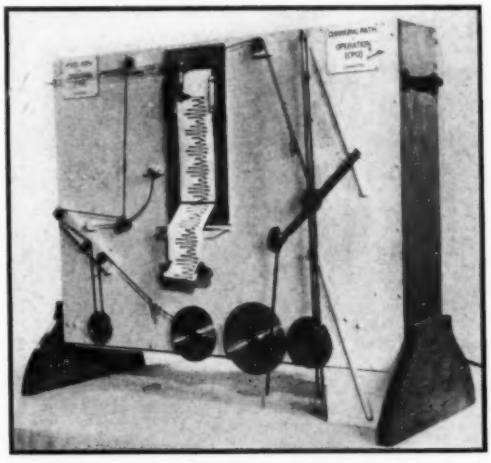

FIG. 1. Motor driven model for the demonstration of square-law, screen grid, and suppressor grid modulators, as well as fundamental types of frequency converters.

[1] H. Stockman, "Superheterodyne converter terminology," Electronics (November, 1943).

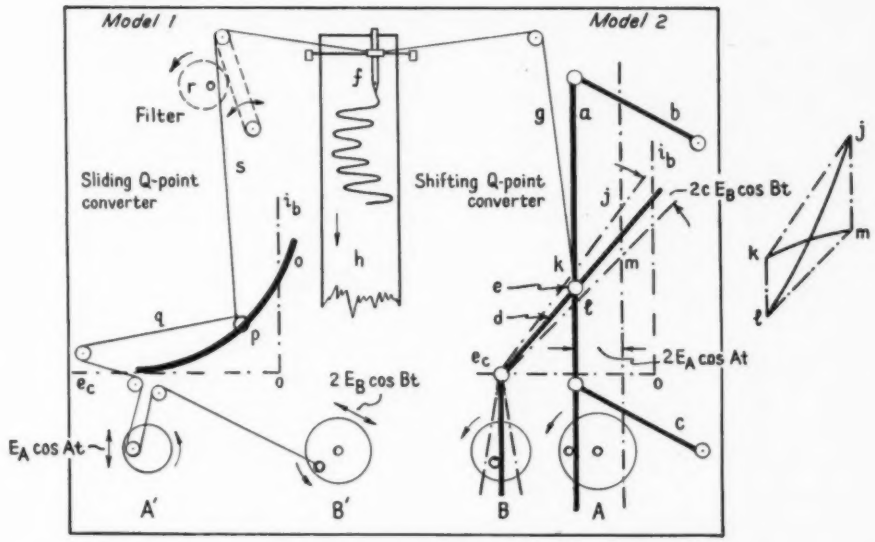

FIG. 2. Simplified drawing showing the design of mechanical FPO and CPO converters. The recording pen can be shifted from one model to the other.

cies such as the lower frequency $(A-B)/2\pi$ and the higher frequency $(A+B)/2\pi$. Still it may not be utilized as a frequency converter but as a modulator. The difference between a converter and a modulator lies in principle in the sorting mechanism on the output side, i.e., in the filter properties of the load.

Two technical terms concerning the linearity of mixers are of intermediate interest. A *linear mixer* or *adder* is a mixer that does not produce any product term. A *non-linear mixer* or *multiplier* is a mixer that produces one or more product terms and therefore is the type of mixer to be used in a frequency converter. Frequency converters may be classified after the type of non-linearity employed.

It is well known that product terms in amplifiers may be avoided if the conditions of operation are so chosen that the quiescent point, or Q point, remains in a fixed position. It is, therefore, to be expected that product terms are created, if the conditions of operation are so chosen, that the Q point is not maintained in a fixed position. In frequency converters and other modulating devices the B source determines the mode of movement of the Q point in an output current *versus* input voltage diagram in one of two possible ways; both are of great practical importance. In the so-called fixed path of operation, FPO, converters the Q point moves or slides* along a fixed path of operation, which necessarily must be curved. A square-law current-voltage characteristic, for example, may be utilized as such a path of operation. In the so-called changing path of operation, CPO, converter the Q point moves or shifts* instantaneously from one current-voltage characteristic to the next in such a way that the path of operation becomes curved. It is equally right to consider the Q point to be located on a given characteristic, which tilts back and forth, controlled by the B voltage. It is of interest to note that even if this characteristic is a straight line, frequency conversion results. The path of operation has a peculiar shape, as can be seen from Fig. 7, *a* and *b*. The reason for this shape will be made clear in the discussion of the mechanical model.

The FPO converter has a non-linearity of "static" character, and employs as mixer a crystal, diode, or single input tube. The use of the FPO converter implies the use of network or circuit coupling on the input side; the two e.m.f.'s

* The terms "sliding Q-point converters" and "shifting Q-point converters" may be used as alternatives to the terms suggested above. Some engineers object to a terminology founded on a moving Q point, as this point is fundamentally defined as a point at rest. The concept of a moving Q point is, however, adopted in the power-tube technique.

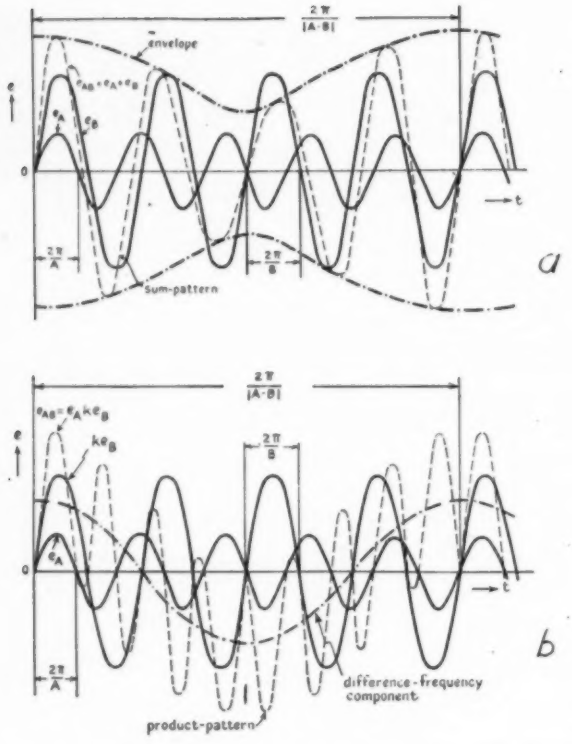

FIG. 3. Sum pattern and product pattern of two sinusoidal waves of different amplitude and frequency.

e_A and e_B being added within the same circuit before applied to the mixing device. The necessary product term is created because of the non-linearity of the mixer, the sum of e_A and e_B —the so-called sum-pattern, see Fig. 3*a*—being distorted so that an alternating component following the envelope pulsations of the sum-pattern is produced.

The CPO converter has a non-linearity of "dynamic" character, and employs as mixer a multi-electrode, double input tube. The use of the CPO converter implies the use of electron-coupling between each source and the mixer circuit. The e.m.f.'s e_A and e_B are introduced on separate electrodes projecting into the electron stream of a tube. The necessary product term is caused by the so-called "gate-effect" which is explained later. A product term or product pattern is shown in Fig. 3*b*. No distortion of this pattern by means of rectification is necessary as the pattern involves the difference frequency as an alternating component. In practice there are no such devices as pure FPO converters and pure CPO converters, as the actions are somewhat mixed.

THE FPO CONVERTER

In the mechanical model of the FPO converter, Model 1 in Fig. 2, the more or less square-law characteristic o is formed by a properly bent metal rod. The Q point is represented by a sliding ring p. The movement of the ring is controlled by the wheel A', rotating with A frequency, and the wheel B', rotating with B frequency. The movements are transferred to the ring p by means of a cord q in such a way that an addition of the amplitudes e_A and e_B is obtained. The input to the mixing device is therefore the sum pattern $e_{AB}=e_A+e_B$, shown in Fig. 3*a*. The instantaneous voltage e_{AB} can be written

$$e_{AB}=E_{A\,\max}\cos At+E_{B\,\max}\cos Bt. \qquad (3)$$

$E_{A\,\max}$ and $E_{B\,\max}$ are absolute amplitudes and may be expressed as a resulting amplitude $E_{AB\,\max}$ times a sine or cosine function. To find this function write the angular velocity A as $(B\pm C)$, where C is the angular velocity of the desired difference frequency component. (The adjustment preferred in the model corresponds to a + sign.) The expression obtained has the form

$$e_{AB}=(E_{A\,\max}\cos Ct+E_{B\,\max})\cos Bt \pm E_{A\,\max}\sin Bt\sin Ct \qquad (4)$$

or

$$e_{AB}=E_{AB\,\max}\cos(Bt-\phi), \qquad (5)$$

where

$$E_{AB}=[E_{A}{}^{2}{}_{\max}+E_{B}{}^{2}{}_{\max}+2E_{A\,\max}E_{B\,\max}\cos Ct]^{\frac{1}{2}},* \qquad (6)$$

$$\phi=\tan^{-1}\frac{\mp E_{A\,\max}\sin Ct}{E_{A\,\max}\cos Ct+E_{B\,\max}}, \qquad (7)$$

The amplitude of the sum pattern e_{AB} thus varies with the envelope frequency $C/2\pi$, which is the desirable difference frequency. The wave inside the envelope is in Eq. (5) expressed as being of B frequency with a fluctuation of C frequency. Thus the sum pattern has angle

* This radical may be developed in a series expansion, inviting to practical approximations. See E. L. Chaffee, *Theory of Thermionic Vacuum Tubes* (McGraw-Hill Book Company, Inc., New York, 1933), p. 548.

modulation as well as amplitude modulation. The half-envelope is generally not sinusoidal but approaches sinusoidal form when $E_{A\ \max} \ll E_{B\ \max}$.

It is important to note that the sum pattern does not contain any new frequency components. Although expressed mathematically in the form given by Eq. (5), it still contains two frequencies only: $A/2\pi$ and $B/2\pi$. The calculation involved points out the fact that the sum pattern has C frequency pulsations, so that *if rectification is applied*, the new frequency component C will be available. Thus, assuming square-law rectification,

$$i = Ke_{AB}^2$$
$$= \cdots + 2KE_{A\ \max}E_{B\ \max} \cos At \cos Bt, \quad (8)$$
$$= \cdots + KE_{A\ \max}E_{B\ \max} \cos (A-B)t. \quad (9)$$

Here i is the output alternating current from a crystal, diode, triode, or multielectrode type of tube, and k a proportionality constant of dimension mhos/volt. e_{AB} has the form given in Eq. (3).

The fact that the FPO converter yields the product term in Eq. (8) is of general significance. The product pattern in Fig. 3*b* shows that when the product term exists, an alternating component of difference frequency $|A-B|/2\pi$ exists as well.

If the B source is treated as a part of the converter, the concept of variable admittance or transadmittance is more helpful than the concept of a sum pattern plus rectification. Assume a tube with a transadmittance or transconductance g_m at the original Q point. The transadmittance variation due to the fact that the path of operation is curved may then be written

$$(g_m)_{\text{inst}} = g_m + \Delta g_m \cos Bt \quad (10)$$
$$= g_m + CE_{B\ \max} \cos Bt, \quad (11)$$

where C is a proportionality constant of dimension mhos/volt. This relation is exact only if the characteristic is parabolic. The plate current component of interest for frequency conversion is

$$(i_p)_{\text{inst}} = (g_m)_{\text{inst}}e_A$$
$$= \cdots + CE_{A\ \max}E_{B\ \max} \cos At \cos Bt, \quad (12)$$
$$= \cdots + \tfrac{1}{2}CE_{A\ \max}E_{B\ \max} \cos (A-B)t. \quad (13)$$

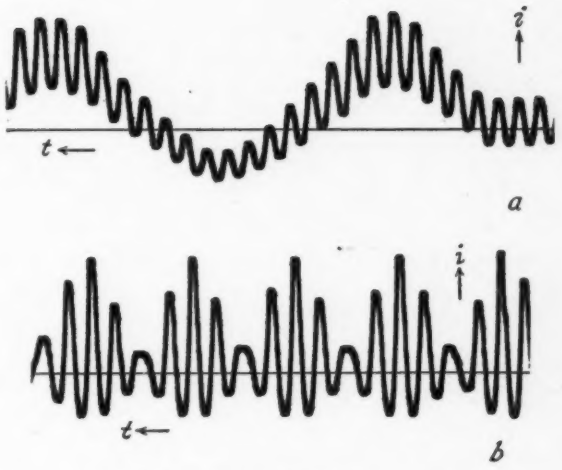

FIG. 4. Recordings obtained with model 1. Both curves represent modulation, but with the chosen A/B ratios curve *a* is of interest for modulation output and curve *b* of interest for conversion output.

This expansion indicates how the sum and difference frequency components are created. A comparison of Eqs. (9) and (13) shows that $C = 2K$.

Figure 4 shows two typical curves obtained with model 1. In Fig. 4*a*, $B \ll A$ so that the output current has the form to be expected from a "square-law" modulator. In Fig. 4*b*, B is increased so that $A \doteq B$. This is the case of interest for frequency conversion. For comparison the curves in Fig. 3*a* and *b* may be obtained, via a mechanical "filter," which cancels the B-frequency component. Such a device r, dotted in Fig. 2, may have the form of a specially shaped disk rotating with B frequency. It automatically absorbs the length variations of the cord s when $E_{A\ \max}$ = constant. During converter operation the pen will be acted upon mainly by cord-length variations caused by the variation in slope value along the characteristic.

Although this discussion is not extended to adjustments of the models for class C operation, that type of operation is naturally of great interest, in particular for centimeter wave receivers with diode mixers.

THE CPO CONVERTER

The fundamental principle for mixer and converter tubes with "dynamic non-linearity" involves the use of two consecutive control grids

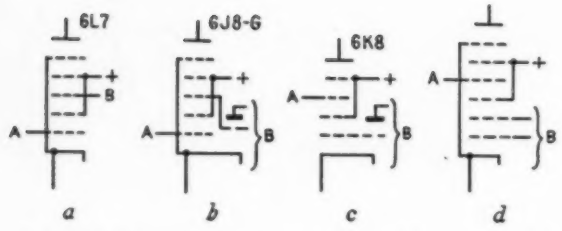

FIG. 5. Mixer and converter tubes with outer-grid injection (a, b) and inner-grid injection (c, d). Fundamentally all devices utilize CPO conversion.

in the same electron stream, all other electrodes being kept at fixed potentials. The result of the consecutive grid arrangement is a pronounced gate effect,[2] the two grids periodically opening up in phase or out of phase with the periodicity $(A-B)/2\pi$. As soon as the slope $\partial i_b/\partial e_1$ of one control grid is a function of the voltage on another control grid, a new term, the product term, with a factor involving $\partial^2 i_b/\partial e_1 \partial e_2$, will show up (subscripts 1 and 2 refer to the consecutive control grids, which do not necessarily follow in the order 1–2). The gate effect is predominantly either a transadmittance gate effect or a current division gate effect, but it is not always necessary to know if the one effect or the other is utilized. The result can in both cases be expressed as a transadmittance or transconductance variation.

The transadmittance gate effect, as produced by the oscillator voltage, is predominant in inner grid injection IGI tubes, such as the ones shown in Fig. 5*c* and *d* (the oscillator grid is closer to the cathode than the signal grid). The current division gate effect is predominant in outer grid injection OGI tubes, such as the ones shown in Fig. 5*a* and *b* (the oscillator grid further away from the cathode than the signal grid). In the tubes shown the control grids are separated by screen grids and the various electrodes operated with suitable potentials, so that as far as possible such direct interaction as space-charge coupling is avoided. The ideal aimed at is fundamentally no coupling between the sources feeding the variational potential electrodes, and sufficiently strong coupling between each one of these sources and the output circuit (idealized electron coupling).

The conditions under which a product term is created in gate-effect tubes will now be considered with the aid of the geometrical representation in Fig. 6*a*. This figure is general and applies to IGI as well as OGI tubes. The treatment is somewhat simplified as far as practical operation of mixer and converter tubes is concerned. Straight line characteristics have been chosen to illustrate the fact that rectification due to curved characteristics is not required for non-linearity.

Assume the direct voltage on a control electrode 2 constant and equal to e_2'' and the total voltage on a control electrode 1

$$e_1 = \bar{E}_{cc} + E_{1\,\max} \cos \omega_1 t. \tag{15}$$

(1 and 2 do not define the position of respective electrodes in the tube.) With $\bar{I}_b$ as a notation for the direct current $g_{mQ}(\bar{E}_{cc} - \bar{E}_c)$, traced out by the Q point under direct current conditions, the equation for the straight line characteristic e_2'' becomes

$$i_b = g_{mQ} e_1 - g_{mQ} \bar{E}_c, \tag{16}$$

which for the e_1 value of Eq. (15) yields

$$i_b = \bar{I}_b + g_{mQ} E_{1\,\max} \cos \omega_1 t. \tag{17}$$

So far the action of the device is the action of a distortion-free amplifier. If now the direct voltage e_2'' on control electrode 2 is caused to vary periodically with the frequency $\omega_2/2\pi$ between the values e_2''' and e_2', the slope of the straight line, or transconductance, will have the instantaneous value

$$\begin{aligned}(g_m)_{\text{inst}} &= g_{mQ} + \Delta g_{mQ} \cos \omega_2 t, \\ &= g_{mQ} + k' E_{2\,\max} \cos \omega_2 t.\end{aligned} \tag{18}$$

It is then assumed for simplicity that the transconductance variation is proportional to the voltage variation. The equation for the straight line characteristic now becomes

$$i_b = (g_m)_{\text{inst}} e_1 - (g_m)_{\text{inst}} \bar{E}_c \tag{19}$$

which for the e_1 and $(g_m)_{\text{inst}}$ values given in Eqs. (15) and (19) becomes

$$\begin{aligned}i_b = \bar{I}_b &+ g_{mQ} E_{1\,\max} \cos \omega_1 t \\ &+ k' E_{2\,\max} (\bar{E}_{cc} - \bar{E}_c) \cos \omega_2 t \\ &+ k' E_{1\,\max} E_{2\,\max} \cos \omega_1 t \cos \omega_2 t.\end{aligned} \tag{20}$$

The tilting back and forth of the characteristic does not under presumed conditions contribute any d.c. component. The second and third terms

[2] H. Stockman, J. App. Phys. **14**, 645–658 (1943).

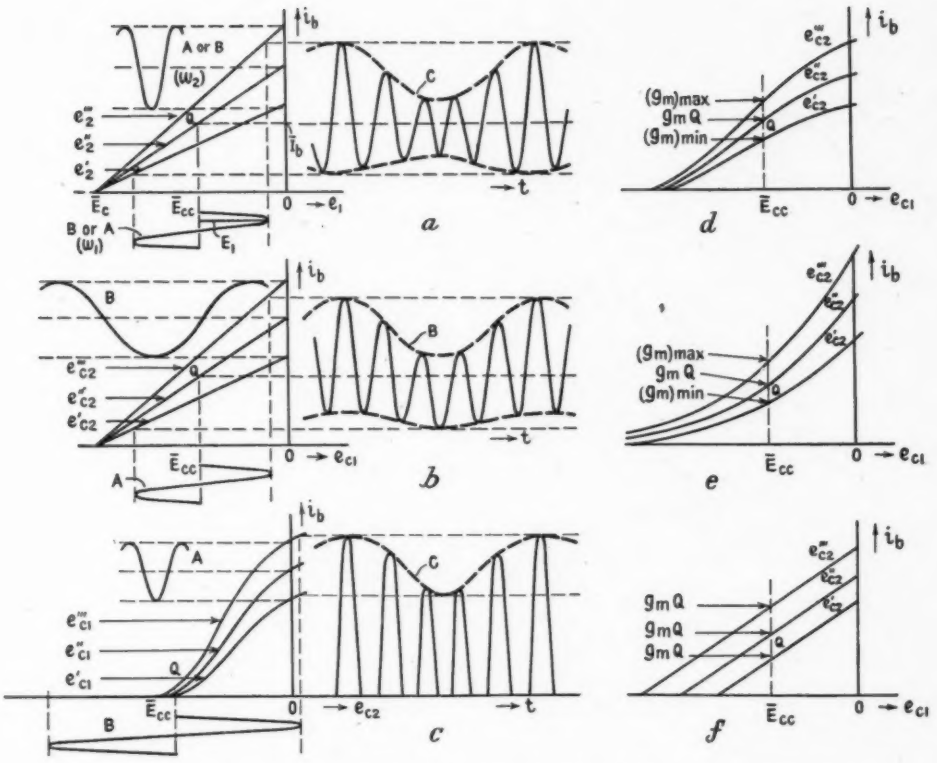

FIG. 6. The working principle for CPO devices is shown in class A operation in *b* and class C operation in *c*. Conditions for non-linear and linear mixing are demonstrated by Figs. *d*, *e*, and *f*.

are carried through due to the amplifier action of the device. The last term is the desired product term, which yields the sinusoidal components

$$\tfrac{1}{2}k'E_{1\,\max}E_{2\,\max}\cos(\omega_1+\omega_2)t + \tfrac{1}{2}k'E_{1\,\max}E_{2\,\max}\cos(\omega_1-\omega_2)t. \quad (21)$$

A rough plot of the total output wave is shown to the right in Fig. 6*a*. This wave will gradually change character if the components in Eq. (20) are filtered out one by one. Finally, when only the last term remains, the wave will degenerate to the shape of a product pattern. Depending upon how the filtering is done, the device of Fig. 6*a* may be used to produce either modulation or conversion. With the relative values of A and B chosen as in the drawing ($A \doteq B$), it is to be expected that the device is intended for frequency conversion. For comparison the same device has been shown in Fig. 5*b* with considerably increased relative difference between A and B. B now represents a low frequency wave (audio or video frequency). It is to be expected that the device in Fig. 6*b* is intended for modulation. $e_1 = e_{c1}$ here represents the voltage on the first grid, so the device is representative for screen-grid or suppressor-grid modulation.

Still another application to the general case is shown in Fig. 5*c*, the close approximation $A \doteq B$ indicating conversion as the main purpose of the device. This application is of great practical interest, as class C operation is employed with a large oscillator swing on an OG1 tube. [Equation (20) shows that the desired output increases with the oscillator amplitude.] The gate effect is not any more the only cause of over-all non-linearity, as the characteristics are curved, the complete analysis of the plate current now being rather involved.

Figure 6*d* shows how the characteristics in Fig. 6*a* may look like in a practical, not idealized case. Figure 6*e* shows another group of tube characteristics, obtained from laboratory measurements. It is interesting to note that the gate effect here controls the plate current to less

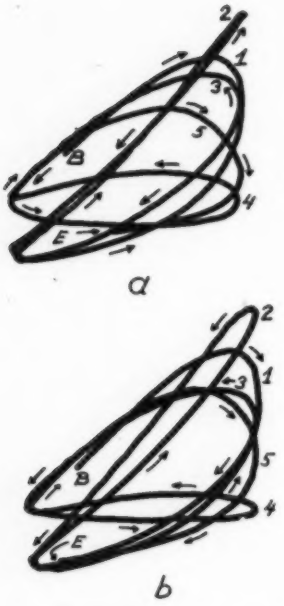

FIG. 7. *a*. Unretouched photograph of the *Q*-point trace of model 2 during a complete i–f cycle, the shift from clockwise to anticlockwise motion corresponding to the phase reversal in a product pattern. *b*. Same trace a few i–f cycles later.

extent than in Fig. 5*d*, as the curves are displaced vertically. This condition is further stressed in Fig. 5*f*, where the gate effect is zero. The mixing may now be said to be *additive*, the tube acting as an *adder* rather than a non-linear mixer. Neither sliding nor shifting of the *Q* point in diagram 6*f* will result in non-linearity. Adders are of great importance in public address systems, pulse circuits, etc.

The essential parts in the mechanical model of the CPO converter are shown to the right in Fig. 2. Here *A* and *B* are two circular disks, rotating with angular velocity *A* and *B*, respectively. A rod *a*, suspended by moving members *b* and *c*, rests against a crank pin in disk *A* and therefore describes a transverse harmonic motion along the axis e_c when the disk *A* rotates. The center of the wheel *A* indicates the point on the axis e_c, determined by the negative grid bias applied to the signal grid. The rod *d* is given a harmonic tilting motion around its mid-position when the disk *B* rotates and the higher the slope of the rod *d*, the higher is the transconductance g_m of the signal grid. The ring *e* in the cross-over point between rod *a* and *d* follows the changing path of operation, and the movements are conveyed via the cord *g* to the pen *f* for recording. The paper strip *h* is pulled downwards by the same motor (1/30 hp) that drives the disks *A* and *B*. The proper relative speeds are obtained by means of suitable gears on the backside of the board and the speed of the main shaft (approximately 6 r.p.m.) is maintained constant by means of a geared-up flywheel. The working parts are held in proper positions by springs not shown in the figure. The area *jklm* covered by the ring is shown somewhat enlarged to the right. When the wheels *A* and *B* are in phase the ring will follow the path *jl* more or less, so that a large variation in vertical ordinate (i.e., plate current) is conveyed to the recording pen. When the wheels *A* and *B* are 180° out of phase, the ring will follow the path *km* more or less, so that a small variation in vertical ordinate (i.e., plate current) is conveyed to the recording pen. The result is a curve, similar to the one shown in Fig. 6*a*, containing the desired difference frequency component. (Errors in the recorded curve due to variations in speed of the main shaft are practically eliminated because the paper movement is obtained from the main shaft.) If the movements of the rings are recorded by means of a camera, the peculiar shapes of the paths of operation in model 2 may be studied more in detail. Figure 7*a* shows a photo of the CPO-converter *Q* point, as it traces out a complete

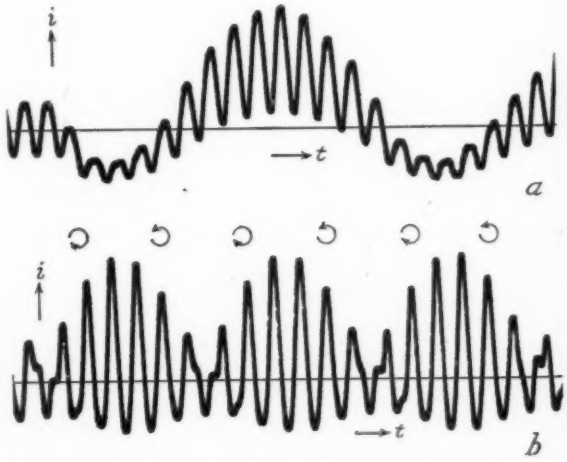

FIG. 8. Recordings obtained with model 2. Both curves *a* and *b* represent modulation; the large *A*/*B* ratio in *a* indicates use as modulator, the small *A*/*B* ratio in *b* indicates use as converter.

i-f cycle. The first loop is described clockwise, the second is merely a straight line, the third and fourth go anticlockwise, and the fifth again clockwise. There are two phase shifts per i-f cycle, corresponding to the two phase shifts in the product pattern, Fig. 3*b*. Figure 8*b* shows where the phase shifts are located on the recorded curve (see the small circular arrows on top of figure; the shifts take place in between the arrows). Depending upon the exact value of A/B the Q-point trace is repeated already the following i-f cycle, or first after a certain finite number of i-f cycles, or, may be, first after an infinite number of i-f cycles. The gradual change in the trace in case of A/B being an irrational number is indicated by Fig. 7*b*, obtained a few i-f cycles later than the trace shown in Fig. 7*a*.

The phase shifts in the Q-point movement prove the multiplicative nature of the action; it is equally difficult to build a linear amplifier with two consecutive variational voltage grids as to make the model trace the loops without going through the phase shifts.

Figure 8 shows two curves *a* and *b*, obtained with model 2 with different frequency ratios A/B. Curve *a* is valid for $B \ll A$ and demonstrates the case of suppressor or screen grid modulation. Curve *b* is obtained with $B \doteq A$ to demonstrate the case when frequency conversion is of interest.

Naturally the use of the recorded curves for mathematical checking requires that corrections are made for various errors due to insufficient precision in the mechanical design. With these corrections the curves may be of interest for Fourier analysis.

CONCLUSION

It has been shown that conventional devices for frequency conversion may be classified as FPO converters and CPO converters. The action of these two fundamental types of converters can be explained by means of mechanical models, such as the ones described. Whether a particular device acts as a modulator or a converter is in principle a question of the choice of output impedance. The models may be used to demonstrate modulation and, especially in case of an added mechanical filter, conversion. It is desirable that models of this type be so designed that the operation can be extended to class C, as such operation is of great practical value.

The recordings shown in the figures hint the use of models such as the one described for investigation and demonstration of the action in various types of modern converters. With some ingenuity, the mechanical design may be extended to permit investigation and demonstration of such phenomena as undesired couplings of various kinds. In addition, analogs to electrical filters may be added and switched in and out to demonstrate the dependence of the output wave form of the individual frequency components. From a pedagogical point of view it may be of interest to mention that the model has given good results in classroom work as students with limited background in electronics quickly grasp the fundamental ideas by watching the movements of the sliding rings.

The author wishes to thank the faculty members of Cruft Laboratory for valuable suggestions concerning the material covered.

The Formation of Bubbles*

ROBERT B. DEAN
Stanford University, Stanford University, California
(Received December 22, 1943)

Extreme values for the negative pressures and the degrees of superheat which water will withstand without forming bubbles are contrasted with the ease of forming bubbles by vibration or by the turbulent flow of liquids. The subject of bubble nuclei is briefly reviewed, and it is pointed out that such nuclei usually function by virtue of sorbed or trapped air which can be removed, rendering the nuclei ineffective. Technique for avoiding extraneous bubble nuclei is presented with some experiments on the formation of bubbles by mechanical action. It is pointed out that free vortices in liquids produce sufficient tension to rupture the liquid, and it is suggested that mechanical disturbance produces bubbles *only* in such vortices and not by general pressure lowering in sound waves.

THE formation of bubbles within liquids is a subject which has received surprisingly little attention from scientists. This is due partly to the fact that bubble formation is a non-equilibrium process not amenable to thermodynamic treatment. In addition, the general prevalence of extraneous bubble nuclei in aerated liquids and on ordinary surfaces which promote boiling and effervescence has led to a lack of realization of the problem. However, there are several problems in heat transfer and distillation where bubble formation is desired, and there are other problems in hydraulics and pressure physiology where bubble formation is to be avoided if possible.

The fundamental difficulty of bubble formation lies in the law relating pressure, surface tension, and bubble diameter.

$$P=2s/r. \tag{1}$$

P = pressure inside minus the pressure outside of the bubble, s = surface tension of the liquid, r = radius of the bubble. For pure water $P=1$ atmosphere when $r=1.42$ microns (0.00142 mm) at 20°C. If the surface tension were constant down to molecular dimensions the excess pressure inside the bubble would be 7500 atmospheres when $r=1.9$A, the mean diameter of a water molecule. Another way of looking at the same thing is to note that in order to form a bubble *de novo* inside a mass of liquid requires that a number of adjacent molecules must simultaneously obtain sufficient kinetic energy to overcome the forces of attraction between them. Except in the region of the critical point only a small fraction of the molecules have energies of this magnitude and the probability of a number simultaneously obtaining sufficient energies for the formation of a bubble is exceedingly minute.

There have been a few theoretical treatments of the probability that random thermal motion of the molecules will form a bubble.[1,2] The results of the theory are not very useful in practical cases as they lead to the conclusion that bubbles are not likely to form in liquids without many degrees of superheat or enormous negative pressures. The theory is qualitatively confirmed in special cases a few of which are quoted below.

Kenrick, Gilbert, and Wismer[3] heated water in small, clean capillaries. They were able to heat water to 270°C at atmospheric pressure. Steam pressure at this temperature is 54 atmospheres absolute. Kenrick, Wismer, and Wyatt[4] were able to saturate water with oxygen, nitrogen, or carbon dioxide at 100 atmospheres and then reduce the pressure to 1 atmosphere without producing bubbles. Dixon[5] repeated an experiment,

* The work described in this paper was done under a contract, recommended by the Committee on Medical Research, between the Office of Scientific Research and Development and Stanford University.

[1] W. Doring, Zeits. f. physik. Chemie **B36**, 371 (1937); **B38**, 292 (1937).
[2] R. Furth, Proc. Camb. Phil. Soc. **37**, 252 (1941).
[3] F. B. Kenrick, C. S. Gilbert, and K. L. Wismer, J. Phys. Chem. **28**, 1297 (1924).
[4] F. B. Kenrick, K. L. Wismer, and K. S. Wyatt, J. Phys. Chem. **28**, 1308 (1924).
[5] H. H. Dixon, Proc. Roy. Soc. Dublin **NS14**, 229 (1914).

originated by Berthelot, in which a closed tube is completely filled with water, by heating to expand the water, thus dissolving the small residual bubble left when sealing off the tube. On cooling, the water did not break away from the walls until the pressure inside the tube was minus 150 atmospheres (the pressure was calculated from the respective coefficients of thermal expansion and compressibility of water and glass). Plant sap, nearly saturated with air at room temperature, withstood 207 atmospheres of negative pressure before rupturing. Similar experiments were done by Meyer[6] who performed the experiment in a spiral manometer and measured negative pressures as great as 30 atmospheres with water and 40 atmospheres with ether.

Many people have found difficulty with the concept of negative pressure* or tensile strength of liquids. It is generally taught in elementary physics that a liquid cannot be "sucked up" to a height greater than the barometric height for that liquid. Nevertheless, there are many experiments such as Dixon's quoted above[5] which prove that a quiet liquid that is not exposed to any gas surface has great cohesion. Another example of a liquid under tension is occasionally met with in constructing barometers. Clean mercury in a clean tube will often stick at the top of the tube, and require a tap on the tube to break the adhesion between the mercury and the glass. Vincent[7, 8] reviews the literature concerning liquids under tension and describes two additional methods for measuring the cohesion of liquids.

BUBBLE NUCLEI

The problem of effervescence of a liquid supersaturated with gas is strictly analogous to the problem of bubble formation in superheated liquids or in liquids under negative pressure. A bottle of carbonated water saturated with CO_2 at 2 to 3 atmospheres, if left quiet for some time before opening and opened without agitation of the contents, will produce few or no bubbles, although shaking the bottle produces copious effervescence. We have carried out many experiments which show that water, supersaturated with a gas, will not produce bubbles unless (a) there are gas particles available below the surface on dust particles or other contamination or (b) the water is subjected to mechanical shock.

It is comparatively easy to eliminate bubble formation due to cause (a), gas on contaminating surfaces, and so be able to study cause (b), mechanical shock. Glass, if cleaned in a hot acid cleaning solution and kept wet, will be free from gas surfaces. Tomlinson[9–11] in a series of papers from 1867 to 1873 presented most of the facts now known about bubble nuclei. He showed that either flaming or cleaning with methylated spirits of wine was an effective way of removing bubble nuclei from solid surfaces. His work on the effect of dirty surfaces deserves better study. We find that boiling out or partial evacuation of water, followed by quiet standing for one or more days, usually removes bubble nuclei from surfaces, presumably by dissolving the gas remaining on solid surfaces.

A number of substances have been tested for their ability to furnish bubble nuclei. The substances tested are listed in Table I together with the cleaning treatment. In every case we were able to remove bubble nuclei by suitable treatment. The various substances were placed in heavy test tubes, covered with water and evacuated to about 50 mm of mercury with an aspirator pump. Whenever a substance showed no bubbles on evacuation, we assumed it was free of bubble nuclei. Then the tube was struck a sharp blow. This always produced a swarm of bubbles proving that dissolved air was available for bubble formation.

A commonly held theory of the action of boiling chips supposes that edges or points promote bubble formation, although Tomlinson[9] showed that this is not generally true. Dorsey[12] pointed out that edges and points which are wet by water could not act as centers to promote quiet boiling. We have confirmed this fact. A glass cover slip broken under water does not promote bubble

[6] J. Meyer, Zeits. f. Electrochemie **17**, 743 (1911).
* A pressure of minus two atmospheres absolute corresponds to minus three atmospheres gauge pressure. Negative pressure can only be realized in gas-free systems containing only liquid and solid phases.
[7] R. S. Vincent, Proc. Phys. Soc. London **53**, 126 (1941).
[8] R. S. Vincent, Proc. Phys. Soc. London **55**, 41 (1943).
[9] C. Tomlinson, Phil. Mag. [4] **34**, 136, 229 (1867).
[10] C. Tomlinson, Proc. Roy. Soc. London **17**, 240 (1869).
[11] C. Tomlinson, Phil. Mag. [4] **45**, 276 (1873).
[12] N. E. Dorsey, Phys. Rev. **55**, 594 (1939).

TABLE I. Substances tested as centers for bubble formation at 50 mm Hg under water partially saturated with air.

Substance	Bubble nuclei present before cleaning	Cleaning treatment	Bubble nuclei present after cleaning
Glass	Yes	Hot H_2SO_4 plus KNO_3	No
Carborundum	Yes	Boiled and cooled under water	No
Mineral oil floating on water	No	None	
Mineral oil plus stearic acid floating on 0.1 *N* NaOH	No	None	
Sugar crystals	Yes	Recrystalized from solution	No
Gelatine granules	Yes	Soaked overnight in water	No
Fibrin	Yes	Soaked overnight in water	No
Cellophane	Yes	Boiled and soaked in water	No
Parafin on glass	Yes	Soaked overnight in water at 4°C	No
Lanolin on glass	Yes	Soaked 2 days in partially degassed water at 4°C	No
Lanolin emulsion prepared from dioxane solution	No	None	
Rubber	Yes	Boil or soak in partially degassed water	No
Aluminum tristearate (technical)	Yes	Soak in partially degassed water	No
Aluminum distearate (technical)	Yes	Soak in partially degassed water	No

formation in water at low pressures. Neither does boiled-out carborundum powder favor bubble formation in water although it is widely used for boiling chips because of its sharp points!

Dorsey[12] suggested that surfaces which are not wet by water would promote quiet boiling. A study of bubble formation in boilers by Jacobs[13] showed that bubbles were initiated by relatively few points on the surface of the plate and that the number of these loci decreased with continued boiling. A graphite point for boiler tubes which promotes bubble formation is mentioned by Jacobs. Henrici[14] found that even graphite was useless for promoting bubbles if outgassed by heating and quenched in water. Charcoal treated the same way promoted boiling but not room temperature effervescence, according to Tomlinson.[11] We have been able to find only one other reported case of a permanent center for boiling in a closed system. Degassed rattan is reported[15] to promote the boiling of SO_2 in sealed refrigerator coils for periods as great as five years.

All other promoters of boiling or effervescence probably have had sorbed air on the surface or trapped air in capillary spaces. Sorption of gases on surfaces shows marked hysteresis[16] and it may require several cycles of sorption and desorption to replace air on a surface by water. Once sorbed air is removed there is no evidence that it will be sorbed again from solution in liquids. The liquid molecules are sorbed on the surface in preference to the more dilute gas molecules.

Although water is commonly supposed not to wet surfaces on which it has a contact angle greater than 90°, the difference between advancing and receding contact angles is taken as a clear indication that water is sorbed on these surfaces.[17] We have found that lanolin forms a surface that is very hard to free from bubble nuclei. Furthermore, bubbles appear to stick to lanolin-coated surfaces under water. However, it is possible to remove bubble nuclei from a test tube coated inside with lanolin by filling it with water, partially evacuating, and then letting it stand for several days. After this treatment, bubbles will not form on evacuation. However, if the lanolin is exposed to air for a moment by inclining the tube, bubbles will afterward form on that part of the surface which had such brief contact with air.

Although a sorbed monolayer of gas would not be expected to promote bubble formation, there is considerable evidence for multilayers of sorbed nitrogen on many surfaces.[18] These multilayers of gas are on the outside very little different in state from free gas and should form favorable nuclei for gas or vapor to collect upon from supersaturated solutions.

[13] M. Jacobs, Mech. Eng. **58**, 643, 729 (1936).
[14] M. C. F. Henrici, Phil. Mag. [4] **45**, 183 (1873).
[15] L. A. Phillip and B. E. Tiffany, Refrig. Eng. **25**, 140 (1933).
[16] J. W. McBain, *Sorption of Gases and Vapors on Solids* (Routlidge, London, 1932), pp. 92–94.
[17] G. Mac Dougal and C. Ockrent, Proc. Roy. Soc. London **A180**, 151 (1942).
[18] P. H. Emmett, *Advances in Colloid Science* (Interscience Publishers, Inc., New York, 1942), p. 1.

It can easily be shown that mechanical agitation forms bubbles in saturated or supersaturated bubble-free systems. This has been found repeatedly with ultrasonic radiation.[19] The mechanical agitation of quiet "soda water" is another example. Marine propellors cavitate at high speeds forming a vortex trail of bubbles and in some cases producing destructive corrosion of the propellor.[20] Venturi tubes cavitate when the pressure in the throat falls to the vapor pressure of water. Cavitation occurs in the turbulent region beyond the throat, where the tube is expanding.[21, 22]

Bubbles can also be produced in evacuated water in thick walled test tubes by a blow on the side. A glass marble rolling in a tube full of water produces a swarm of bubbles when the marble strikes the end of the tube.

The usual explanation of the formation of bubbles by mechanical action assumes that bubbles will form when the pressure is reduced to the pressure of water vapor, either by a sound wave or by Bernoulli's principle, in a constricted tube. However, calculations of the minimum pressure produced by supersonic waves show that less than one-tenth of the energy necessary to produce a pressure as low as the vapor pressure of water will produce cavitation.[23]

Similarly, cavitation has been produced by metal plates vibrating with a frequency of 8500 cycles per second and an amplitude of 0.01 mm.[24] The calculated pressure lowering is 0.8 atmosphere. Saw-tooth waves, however, would produce a greater maximum pressure at the same fundamental frequency.

Dixon's experiment[5] proves that water can withstand a tension of more than 150 atmospheres. There is no *a priori* reason why pressure waves of a much lower order of magnitude should cause cavitation. Since the frequency of collision of water molecules is of the order of 10^{11} per second, a dynamic tension with a frequency of 10^4 seconds should not be significantly different from a static tension. One should therefore not look for the origin of bubbles produced by mechanical action in the linear tension produced by this action. It has sometimes been supposed that cavitation occurs when some part of the system moves faster than the speed of sound in water. The experiment quoted in the previous paragraph[24] shows that this explanation cannot be generally true since the plate was moving at a maximum velocity of only 25 cm per sec.

Hatcher and Sage[25] showed that turbulence reduced supersaturation in hydrocarbon mixtures and suggest that localized regions of low pressure associated with vortices which are widespread in turbulent flow are conducive to the formation of small bubbles.

I would extend this hypothesis and suggest that free vortex motion is probably always responsible for the bubbles formed when liquids are subjected to mechanical disturbance.

The ideal rectilinear free vortex has a pressure at any point, relative to undisturbed liquid, that is inversely proportional to the square of the radius vector of the point.[26]

$$P = -\Gamma^2 d/8\pi^2 r^2. \qquad (2)$$

P is the difference in pressure between the point in question and undisturbed liquid, neglecting hydrostatic pressure; Γ is the circulation; d is the density of the liquid; and r is the radius vector of the point in question. The calculated pressure at the mathematical center of a free vortex is therefore minus infinity. In practice, free vortices have a core which may contain gas or vapor or else liquid moving as a forced vortex. In a forced vortex, the pressure at any point, in a plane perpendicular to the axis, above that in the center is proportional to the square of the radius vector

$$P = w^2 r^2 d/2. \qquad (3)$$

w is the rate of revolution of the vortex. A free vortex is irrotational in the sense that except on

[19] C. Boondy and K. Sollner, Trans. Faraday Soc. **31**, 835 (1935).
[20] L. P. Smith, Trans. A.S.M.E. **59**, 409 (1937).
[21] J. C. Hunsacker, Mech. Eng. **57**, 211 (1935).
[22] L. F. Moody and A. E. Sørensen, Trans. A.S.M.E. **57**, 425 (1935).
[23] R. W. Boyle, G. B. Taylor, and D. K. Froman, Trans. Roy. Soc. Canada **23**, No. 3, 187 (1929).
[24] J. C. Hunsacker, Trans. A.S.M.E. **57**, 423 (1935).
[25] J. B. Hatcher and B. H. Sage, Ind. Eng. Chem. **33**, 443 (1941).
[26] L. Prandtl and O. G. Teitjens, *Fundamentals of Hydro- and Aero-Mechanics* (McGraw Hill Book Company, Inc., New York, 1934), p. 213.

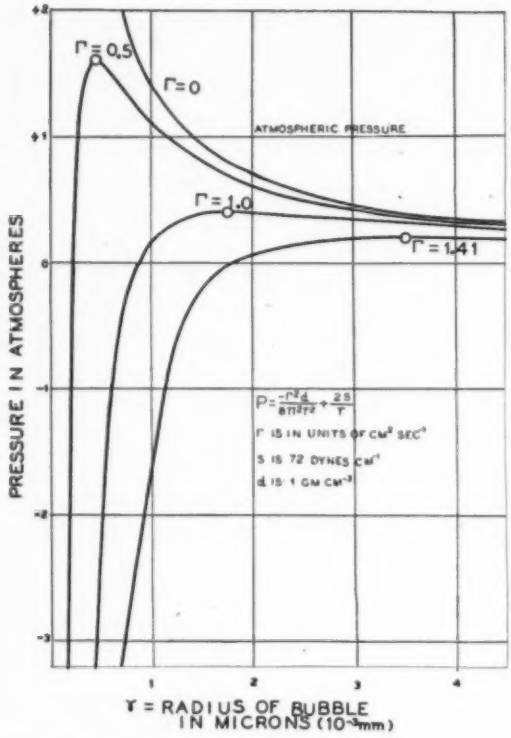

FIG. 1. Pressure on a spherical bubble in water at the center of a vortex of circulation Γ. Maxima are indicated by circles.

the axis the individual particles do not rotate on their own axes. A forced vortex is rotational. There is no complete theory of the formation of vortices that constitute turbulent flow because of the difficulty of the boundary conditions. Several theories of vortex motion in a viscous fluid have been proposed.[27] All agree that the size of the forced vortex core will increase with time. Some theories extrapolate back to a free vortex with no core at zero time. This would produce sufficient tension to rupture the liquid and, if conditions were otherwise favorable, lead to the formation of a core of bubbles. Such a core is actually observed with marine propellors.[28] If the liquid is not nearly saturated with gas or vapor, the minute cavity in the center of the vortex will collapse again, forming part of the core of the vortex.

The pressure inside a bubble at the center of a free vortex is the sum of the vortex pressure and the surface tension pressure. Assuming a spherical bubble (the case of a cylindrical bubble is similar with s/r for the surface tension contribution)

$$P = -\Gamma^2 d/8\pi^2 r^2 + 2S/r. \tag{4}$$

This function is plotted in Fig. 1 for several values of Γ. When P is less than the total gas pressure inside the bubble P_v, the bubble will grow. When P is greater than P_v the bubble will shrink. An inspection of Fig. 1 shows that a free vortex with any circulation can produce a small bubble. If, however, the pressure of the gas plus the vapor P_v is less than the maximum pressure due to surface tension forces, the bubble will remain small and will disappear when the vortex dies out. If the total pressure produced in the bubble P_v is large, then the bubble will be expanded over the maximum in the curve and will expand spontaneously at a rate controlled principally by the rate of diffusion of gas or vapor into the bubble. More active vortices, which have greater circulation, will have lower maxima and will form permanent bubbles at lower values of P_v.

Qualitative observations which support this interpretation of bubble formation have been made in a system which was designed so that high frequency vibrations would be damped out by a rubber diaphragm. A glass tube, 1-cm inside diameter, 2 cm long, was sealed to a 2-mm tube at one end. The other end was closed with a rubber diaphragm, 2 mm thick, held on by a ring clamp. This vessel was filled with water and, once the rubber and glass were freed from bubbles, evacuation to 50 mm Hg produced no bubbles. A blow on the center of the rubber diaphragm produced bubbles if a threshold value of the blow was exceeded. More viscous solutions raised this threshold value. When weak gelatine gels were cast in the apparatus, bubbles would not form until after the gelatine had been ruptured. When a layer of 2 percent gelatine, 4 mm thick, was cast on the diaphragm and covered with water, a blow on the rubber produced bubbles in the water but not in the gelatine. In this last experiment the normal stress in the gelatine was at least as great as in the water, yet the water cavitated, and the gelatine did not. The effect of raised viscosity can best be explained by the fact

[27] H. Bateman, Bull. Research Council **84**, 212 (1931).
[28] J. Metschul, J. Phys. Chem. **28**, 417 (1924).

that turbulent flow requires higher velocities in more viscous solutions.

Mechanical movement of liquids in closed vessels is always hindered by the viscous drag of the walls. Because of this wall effect, it is impossible to produce an ideal pressure wave in a tube in which every particle in a given cross section moves the same distance. This resistance to ideal flow will cause turbulence when water in a tube is set in vibration. In our experiments with a rubber diaphragm over the end of a glass tube, we could detect turbulence by the motion of anisometric particles (red blood cells) when the diaphragm was struck. We found it easier to produce bubbles when the free upward movement of water in the wide tube was restrained by filling the constricted neck partly full of water. Under these conditions, turbulence was also greater. Boondy and Sollner[19] review experience with cavitation produced by ultrasonics. They find that bubbles are usually formed at interfaces, particularly at liquid-liquid interfaces. Reynolds[29] found that turbulence was produced at very low relative velocities at liquid-liquid interfaces. This agrees with the well-known instability of a vortex sheet.

It seems highly probable that most cases of cavitation or bubble formation produced by movement in liquids occur in vortices produced by turbulent motion of the liquids. Vortices will, of course, expand bubble nuclei on dust particles, if any are present, at energies insufficient to cause true cavitation. It is not possible to rule out completely the possibility that simple pressure waves produced by high energy ultrasonic vibration might produce bubbles by a direct pull exceeding the cohesive strength of water. That this does actually occur has not yet been proven.

Since the diffusion coefficients of most gases are so nearly equal, the rate at which gas enters a bubble will be controlled largely by the amount of gas close to the bubble, that is, by the absolute solubility of the gas. We have found that solutions of carbon dioxide in water form bubbles with much less agitation than solutions of air. Metschul[28] also found that CO_2 formed bubbles more easily than N_2, O_2, or H_2, although others have found no significant difference when the liquid is not disturbed.[4] Since CO_2 is about 50 times as soluble as N_2 in water, more will be available near a newly formed cavity and there is consequently a greater probability that the pressure in the bubble will be built up high enough to overcome the surface tension pressure before the vortex decays.

A practical conclusion from this theory of bubble formation is that bubbles can always be produced by active stirring or turbulent circulation of the liquid. This fact is well known though not often intentionally applied in practice. There are dozens of suggestions in the literature for "boiling chips" and bubble nuclei of various sorts to prevent bumping, yet I have found only one reference to the use of agitation to prevent bumping during boiling.[30] However, the use of many boiling chips actually produces considerable turbulent motion of convective streams when flasks are heated from below. Superheating of boilers could be entirely eliminated by suitable forced circulation or other means of producing turbulence in the water. This will be of greater importance in boilers that recycle pure water. Other cases of supersaturation or superheating of liquids may also be cured by suitable agitation or circulation of the liquids.

The author is indebted to Professor L. R. Blinks for some of the experiments reported here as well as for helpful advice and criticism throughout the course of this work.

[29] O. Reynolds, Phil. Trans. **174**, Part 3, 943 (1883).

[30] W. Steinkopf and H. Winternitz, Chem. Ztg. **37**, 40 (1913).

Thermal and Electrical Conductivity of Graphite and Carbon at Low Temperatures

ROBERT A. BUERSCHAPER
Lehigh University, Bethlehem, Pennsylvania
(Received January 6, 1944)

Thermal and electrical conductivities of graphite and carbon were measured at various temperatures in the range between −191°C and 100°C. Thermal conductivity of graphite was found to increase at an increasing rate as the temperature was lowered and two values were always found for Acheson graphite, a longitudinal and transverse conductivity, the latter being about ½ the former. This effect has not been reported for artificial graphite although Wooster reported an anisotropy in natural graphite with respect to thermal conductivity, the values along the axis being about four times that at right angles. X-ray patterns give no evidence of crystalline alignment in Acheson graphite and the explanation of this anisotropy has not been found. The electrical conductivity of graphite increases with rise of temperature as contrasted with the decrease of the thermal conductivity with temperature rise. Thus the Wiedmann-Franz law does not hold, nor is the Lorentz number a constant. Carbon shows no anisotropy. The thermal and electrical conductivities both increase with temperature rise, the thermal conductivity linear, in the temperature range −191° to 100°C.

INTRODUCTION

THE present lack of data on the thermal conductivity of carbon and graphite at low temperatures leads to the undertaking of this work. Graphite occupies a unique position among conductors and non-conductors in that as far as its thermal conductivity is concerned it acts as a metal. The curve of thermal conductivity *versus* temperature for graphite shows an increase in conductivity with a decrease in temperature. As far as the trend of the electrical conductivity is concerned graphite behaves somewhat as an insulator; that is, the electrical conductivity rises with rise in temperature; but in absolute value is much greater than for insulators. Carbon acts as an insulator as far as the trends of its curves of thermal and electrical conductivity are concerned. Both the thermal and electrical conductivity increase with increase in temperature. It was to establish the trend of these curves and the absolute values of the conductivities at low temperature that this work was undertaken.

THEORY OF THE METHOD

The theory of the method was developed and given by Bidwell[1] in a paper on the thermal conductivity of zinc. Equating the heat lost per cm radially from the specimen to the difference in vertical heat flow per cm we have

$$2\pi k_s \Delta T/2.3 \log_{10}\frac{R_2}{R_1}=k_z A\frac{d^2T}{dx^2}.$$

k_s is the thermal conductivity of the Silocel surrounding the specimen at the temperature in question; ΔT the radial drop across the Silocel; R_2 and R_1, the inner and outer radii of the Silocel; k_z, the thermal conductivity of the test rod; A its cross section; d^2T/dx^2, the second derivative of the temperature-distance curves (see Fig. 1).

EXPERIMENTAL ARRANGEMENT AND PROCEDURE

Test specimens were cut from Acheson graphite electrodes both parallel to the electrode (longitudinal specimen) and at right angles to its length (radial specimen), and also from a carbon electrode, both supplied by the National Carbon Company. The specimens were 32 cm long by 2.9 cm in diameter. They were cut in half lengthwise and a 1-mm slot milled the whole length down the center of one of the halves. The specimens were then put back together and soldered in to a heat sink of brass and a doughnut-shaped electric heater fastened to the other end. This was then put into a metal container 39 cm long by 10 cm in diameter and packed with Silocel. The metal container was put into a large

[1] C. C. Bidwell, Phys. Rev. **56**, 594 (1939).

Dewar flask and this flask was then filled successively with water 100°C, ice 0°C, dry ice and alcohol −78°C, and liquid air −191°C, depending on the temperature at which the conductivity was being measured.

The cold junction of the thermocouple was kept in the bath of constant temperature outside the metal container while the hot junction was raised 2 cm at a time up through the slot milled in the specimen. The galvanometer readings give the temperature-distance curve for the specimen and also the radial temperature drop across the Silocel. Plotting the curve of galvanometer deflections *versus* distance along the specimen we can obtain the first and then the second derivative of the deflections with respect to x. Since for small temperature ranges the change in temperature is equal to the galvanometer deflections multiplied by a constant, the ratio of the $\Delta T/d^2T/dx^2$ can be substituted by $\Delta D/d^2D/dx^2$, where D is the galvanometer deflection.

Since the lead wires of the hot junction had to pass through the heater, considerable heat was conducted down these wires and raised the temperature of the hot junction above that which it would normally have. In order to correct for this, couples of different diameter wires were used and then the deflections were plotted against area of the couple wires. These points gave a straight line and the line was extrapolated back to zero cross section to correct for the heat flow down the wires. It was these corrected galvanometer readings which were plotted against distance (x) on specimen. The slopes of these curves were obtained graphically and plotted against distance x down the specimen. The slopes of these latter curves gave values of d^2D/dx^2.

If we plot ΔD *versus* d^2D/dx^2, this should give us a straight line going through the origin and the ratio of $\Delta D/d^2D/dx^2$ needed to obtain k_x (thermal conductivity) can be obtained from this line. These straight lines which were obtained with different energy inputs to the heater were found to go through the origin within the limit of experimental error. A consistent slight shift giving an intercept to the left of the origin was found to

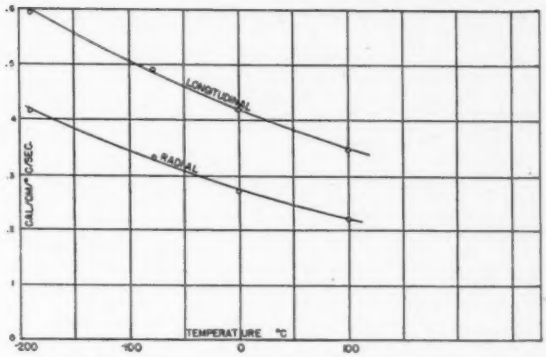

FIG. 2. Thermal conductivity of graphite *versus* temperature.

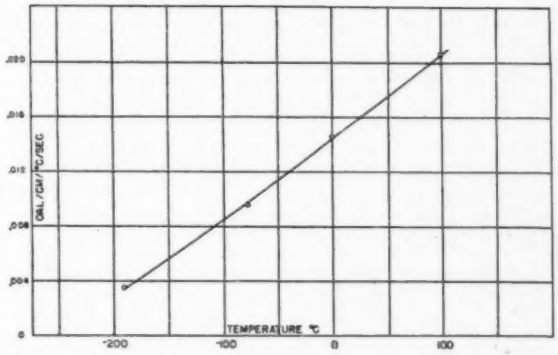

FIG. 3. Thermal conductivity of carbon *versus* temperature.

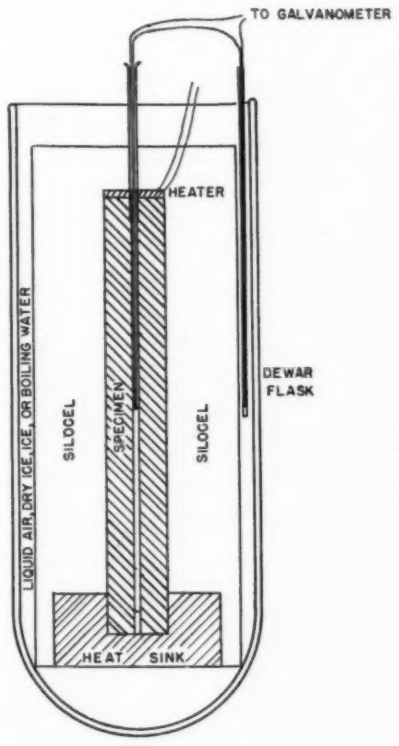

FIG. 1. Diagram of apparatus.

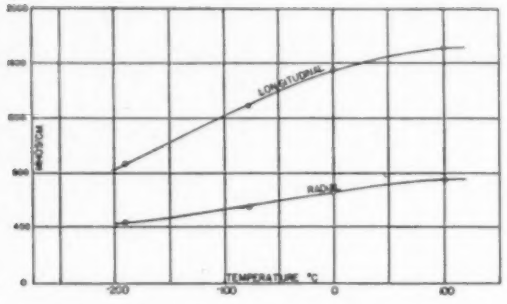

FIG. 4. Electrical conductivity of graphite *versus* temperature.

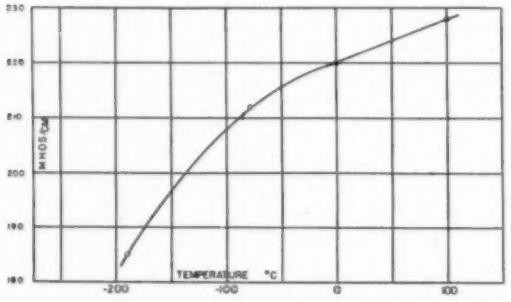

FIG. 5. Electrical conductivity of carbon *versus* temperature.

be due to the heat sink which gives an effect of lengthening the specimen. The heat sink increases the heat flow down the specimen, increasing the gradient in the rod but in the Silocel the temperature modification does not keep pace, the temperature at the outer boundaries of the Silocel being hardly changed. Thus the ΔD's are smaller than they should be since the specimen temperatures are higher. This merely shifts the straight lines to the left. The effect is enhanced by an increase in energy to the heater at the top of the specimen. The slopes of the lines plotted for various inputs to the heater are the same but as the heater energies are increased, the intercepts shift slightly to the left of the origin.

Electrical conductivities were measured in the same specimens. The specimen was brought to the desired temperature by putting it directly into the bath in the Dewar flask and measuring the potential drop across the 10-cm middle portion. Then

$$\rho=\frac{E}{I}\frac{a}{l}; \quad C=\frac{1}{\rho}$$

where a is the area of the specimen, l equals 10 cm, and C equals conductivity.

RESULTS

Figures 2–5 are the curves of thermal and electrical conductivity *versus* temperature. The curves show the longitudinal thermal conductivity of graphite to be almost twice that of the radial conductivity. The values range from 0.35 to 0.59 cal./cm/°C/sec. for graphite (longitudinal) and 0.22 to 0.42 for the radial specimen. For carbon the values range from 0.0037 to 0.021 in the temperature range −191° to 100°C.

The electrical conductivities of graphite range for the longitudinal specimen from 900 to 1700 mhos/cm while for the radial specimen they go from 400 to 700 mhos/cm. There seems to be a tendency toward a flattening of the curve at the higher temperatures. The curve for carbon rises only slightly between −191°C and 100°C going from 180 to 220 mhos/cm.

The above data are in good agreement with the values of the thermal and electrical conductivities for graphite at 0°C as found by Powell and Schofield[2] who have published data on graphite and carbon at the ice point and in the region from 100°C to 2500°C. Their average value of the thermal conductivity for graphite is about 0.34 cal./cm/°C/sec., while the value given in this work is about 0.35 cal./cm/°C/sec. at 0°C.

[2] R. W. Powell and F. H. Schofield, Proc. Phys. Soc. **51**, 153–172 (1939).

Letter to the Editor

Microradiographs and X-Ray Micrographs

ELSIE L. GARVIN
Research Library, Eastman Kodak Company, Rochester, New York
March 1, 1944

AT the present moment, is there any scientific field in which the terminology is becoming so confused as in the growing field of industrial radiography or in which it is so important that action be taken, now, to standardize the terminology? With standardization reached, editors would have an authority to quote and be relieved of needless discussions with authors; indexers for the abstract journals could systematize the present loose and varied headings into meaningful ones, and the users of periodical literature could tell by the title, once again, something of the content of the article.

One article, out of the numerous ones which might be quoted, is used here to illustrate the point. At the start the following distinctions should be firmly fixed in mind.

1. *Microphotography* involves the production of photographs (*usually of large objects*) on a microscopic scale. This should be easy to remember with the present extensive use of microfilm copies of books and periodicals.

2. *Photomicrography* involves the production of enlarged photographs of *small objects*. A magnification of 20× which might be obtained with a camera lens, not involving a microscope, could reasonably be called a photomicrograph.

Carry these definitions in mind and consider the word *microradiography* which appeared in the title of an article by S. E. Maddigan: "The technique of microradiography."[1] From the title it should appear that the author is dealing with radiographs,—of alloys, for example—reduction of these pictures on 35-mm or 16-mm film, and their projection which brings them up to a readable size. Mr. Maddigan, however, is dealing with alloys which have been photographed by means of x-rays, at magnifications of 60× and 80×. Figure 1 is correctly captioned "Photomicrograph of 80 percent Cu, 10 percent Sn, 10 percent Pb at 60×" while Fig. 2 is incorrectly captioned "Microradiograph of 80 percent Cu, 10 percent Sn, 10 percent Pb at 80×." Checking against definitions (1) and (2) it is clear that the author is not writing about a small picture in Fig. 2.

If we are to accept an unfortunate explanation which appeared in the *Transactions of the American Society for Metals*:[2] "Microradiography grew out of the desire to obtain and view radiographic images of heterogeneous objects of small size," then the title quoted above would be correct.

Over long usage in the metal field the term "photomicrograph" has been abbreviated to micrograph. Keeping this popular form, and adding x-ray we then have *x-ray micrograph*, meaning micrography or photomicrography with x-rays. This appears to be a short simple clear term. *Microradiograph* can then be reserved for a radiograph, reduced in size. A good example of these is the microfilms of chest radiographs used at present in military medical branches. *Radiomicrography* is frequently used with the same meaning as x-ray micrography; discussion of the pitfalls in this term can be left to the standardizing authorities. Comparable to x-ray micrograph would be the term *electron micrography*.

Following the above terms comes the confusion in usage of such terms as: *mass miniature radiography, miniature mass radiography*, and *fluorography*. A good definition of *macrophotography* is desirable. Sometimes biologists use this to denote small reductions instead of magnification. Discussion on some of this terminology has recently been appearing in the British journals.[3] Do not forget that we also have both radiography and radiology and varying definitions of these words in the literature.

As a matter of analogy, let us suppose that Mr. Maddigan made some motion pictures of photomicrographs showing the formation of crystal forms. Since he wrote about microradiography he would probably mention this work by the name of *microcinematography*, instead of the correct *cine photomicrography* or *motion picture photomicrography*. The same confusion has occurred in these terms as between microradiography and x-ray micrography. This was discussed by the writer in a note to the editor of the *Journal of the Biological Photographic Association*.[4]

The war has brought the field of industrial radiology to the fore, and the confusion in terminology in the highly technical scientific literature, plus everyday misusage, spreads rapidly in all directions. Once an erroneous term has become popular, it is not easy to eradicate it. Add to the fault of being erroneous, the factor of confusion, and it is plain that it is not possible to make too strong the plea for thought and action on the subject of terminology.

[1] S. E. Maddigan, J. App. Phys. **15**, 43 (1944).
[2] Trans. A. S. M. **29**, 733 (1941).
[3] D. A. Spencer, Phot. J. **83**, 419 (1943); L. V. Chilton, Brit. J. Phot. **91**, 8 (1944), and a comment on Mr. Chilton's letter by H. W. Greenwood, Brit. J. Phot. **91**, 32 (1944).
[4] E. L. Garvin, J. Biol. Phot. Assn. **12**, 80–81 (1943).

Calendar of Meetings

May

5– 6	American Physical Society, Southeastern Section, Atlanta, Georgia
6	American Association of Physics Teachers, Colorado-Wyoming Chapter, University of Colorado, Boulder, Colorado
10–12	American Oil Chemists Society, New Orleans, Louisiana
12–13	Acoustical Society of America, New York, New York
14–16	American Institute of Chemical Engineers, Cleveland, Ohio
17–18	Society of Automotive Engineers, New York, New York
20	Society of Rheology, Polytechnic Institute of Brooklyn, Brooklyn, New York

June

5– 7	Society of Automotive Engineers, Detroit, Michigan
22–25	American Association of Physics Teachers, Cincinnati, Ohio,
23–24	American Association of Physics Teachers, Rochester, New York
23–24	American Physical Society, Rochester, New York
26–30	American Institute of Electrical Engineers, St. Louis, Missouri
26–30	American Society for Testing Materials, New York, New York

July

16–21	American Society of Civil Engineers, Chicago, Illinois
22	American Physical Society, Berkeley, California

Here and There

Bulletin of Mathematical Biophysics

The June, 1944 issue of *The Bulletin of Mathematical Biophysics*, Vol. 6, No. 2, has the following table of contents:

A Note on the Mathematical Biophysics of Ameboid Movements. RALPH BUCHSBAUM, N. RASHEVSKY, AND HENRY E. STANTON.
On a Possible Mechanism for Biological Periodicity. MANUEL F. MORALES.
On the Theory of Cell Division from the Point of View of the Principle of Maximum Energy Exchange. HENRY E. STANTON.
A Note on Neural Nets. H. D. LANDAHL.
Equivalence of the Theories of Nervous Excitation of Hill, Monnier, and Rashevsky. ALSTON S. HOUSEHOLDER.
Book Review—JOSEPH NEEDHAM, *Biochemistry and Morphogenesis.* ALSTON S. HOUSEHOLDER.

Standard Samples of Hydrocarbons

In accordance with the announcement made under date of June 1, 1943 by Dr. Lyman J. Briggs, Director, work was begun at the National Bureau of Standards on July 1, 1943 on the preparation of standard samples of hydrocarbons of known high purity for calibrating analytical instruments and apparatus in the research, development, and analytical laboratories of the petroleum, rubber, and allied industries. In order to expedite the work, and to make available the largest possible number of compounds in the shortest time, only a limited quantity of each hydrocarbon has been prepared and the purity of each has been pushed only to a point that is believed to be amply adequate for the present urgent needs for calibration.

There are now available under this program fifteen hydrocarbons, as given in Table I.

TABLE I.

Compound	NBS standard sample number	Amount of impurity mole percent
n-Pentane	201	0.25 ±0.10
2-methylbutane (isopentane)	202	0.13 ±0.06
n-Hexane	203	0.24 ±0.09
2-Methylpentane	204	0.25 ±0.10
3-Methylpentane	205	*
2,2-Dimethylbutane	206	0.12 ±0.05
2,3-Dimethylbutane	207	0.06 ±0.04
Methylcyclopentane	208	0.25 ±0.09
Cyclohexane	209	0.012 ±0.007
Benzene	210	0.05 ±0.02
Methylbenzene (toluene)	211	0.04 ±0.02
Ethylbenzene	212	0.20 ±0.07
1,2-Dimethylbenzene (o-xylene)	213	0.14 ±0.05
1,3-Dimethylbenzene (m-xylene)	214	0.17 ±0.07
1,4-Dimethylbenzene (p-xylene)	215	0.07 ±0.03

* Not determined; believed to be the same as for 2-methylpentane.

Each of these hydrocarbons is available at the costs indicated in Pyrex glass ampoules, sealed in vacuum, in the following kinds and sizes of containers listed in Table II.

Proper designation is illustrated as follows: An order for 8 ml of cyclohexane, sealed in vacuum in a special Pyrex glass ampoule with internal vacuum "break-off" tip, would be given as Cyclohexane, No. 209–8s. Similarly, an order for 5 ml of 2,2-dimethylbutane, sealed in vacuum in a plain Pyrex glass ampoule, would be given as 2,2-Dimethylbutane, No. 206–5.

TABLE II.

Designation to follow standard sample number	Volume of hydrocarbon	Kind of container	Cost per sample
−5	5 ml	plain ampoule, sealed in vacuum	$3.00
−8s	8 ml	special ampoule, with internal vacuum "break-off" tip, sealed in vacuum	5.00
−25	25 ml	plain ampoule, sealed in vacuum	9.00

For simplification the cost of the various hydrocarbons has been made the same. Prices are subject to change as conditions warrant. The cost includes delivery under government frank in the United States and to Mexico, Canada, Cuba, and United States possessions. For all shipments to other countries, 50 cents postage must be added for each container, and, in addition, 25 cents for insurance or registration of each shipment.

Samples must be paid for in advance, with order. Money orders, checks, etc., should be made payable to the National Bureau of Standards. Payment for foreign orders should be by an international money order or by a check payable through the New York Clearing House or a bank in the United States.

Orders should be addressed to the National Bureau of Standards, Washington 25, D. C., specifying clearly by number and name the hydrocarbons and containers wanted.

New Booklets

Spectrographer's News Letter, Vol. 1, No. 4, March, 1944, features descriptions of the "Quartz mercury lamp for high voltage spark units" as well as "Specific techniques for spectrographic analysis of aluminum and magnesium alloys." Copies can be obtained from the Harry W. Dietert Company, 9330 Roselawn Avenue, Detroit 4, Michigan. (3 pages.)

Modern pH and Chlorine Control, a completely revised 83-page combination handbook and catalog (sixth edition), of value to everyone interested in control of *p*H (acidity and alkalinity), chlorine, phosphates in boiler water, and in water analysis, is available, free upon request, from W. A. Taylor & Company, 7300 York Road, Baltimore 4, Maryland. This booklet is devoted to a simple non-technical explanation of the meaning of *p*H control and the methods for making colorimetric determinations, as well as a technical discussion of the meaning of *p*H control, precautions to be observed, and the application of *p*H and chlorine control to 31 different fields. It also contains a description of Taylor slide comparators for general *p*H and chlorine control, etc.

Ohmite News, January and February, 1944, contain a résumé of "The Edison effect—a first in electronics." Instruments illustrated in these booklets are the Ohmite rheostats, resistors, and tap switches. Ohmite Manufacturing Company, 4835–41 Flournoy Street, Chicago, Illinois, is the publisher. (2 pages.)

Recent Applications of Physics

Prepared by CLARK GOODMAN, Associate Editor

Material to be included in this section should be submitted to Dr. Clark Goodman, Massachusetts Institute of Technology, Cambridge 39, Massachusetts.

Magnetic Defectoscope Railroad rails can be examined in place at speeds up to 15 miles per hour using a recently developed magnetic method.[1] The iron rail is magnetized by a suitably placed coil. Variations in the magnetic field are detected by means of a specially designed vacuum tube. The top of the glass tube is flattened in order to allow the electrodes to be placed as close as possible to the rail. A semicylindrical anode is arranged with its open side toward the flattened top of the vacuum tube. Directly adjoining the glass and coaxial with the anode is a cathode wire filament. The current in this diode remains essentially constant until a defect in the rail is encountered. The resulting discontinuity in current is amplified and its variation observed by means of a recording milliameter synchronized with the rate of scanning. By adjusting the grid bias of the amplifier, the effect of a steady magnetic field can be neutralized and the recorder made to deflect only when a change is encountered. It is reported that the instrument is sensitive to defects amounting to only a few tenths of one percent of the total section of the rail.

[1] Gorelik, Smirnov, and Samarin, Vestn. Metallopron., No. 7, p. 67 (1939).

Production-Line Radiography The cost of apparatus and film has restricted the use of x-rays for product inspection. However, a method has now been developed that makes possible production-line radiography. A high speed camera photographs, on two-inch film, an x-ray image of the product cast on a foot-square fluorescent screen. Using the Westinghouse instrument shown schematically in the adjoining figure, about 300 exposures can be made on a 50-foot roll of film. Special precautions have been taken to safeguard personnel from the radiations.

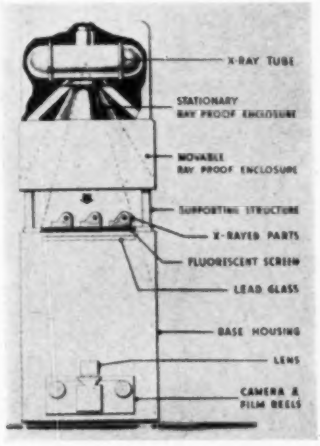

Heterogeneous Plies Aircraft manufacturers are discovering that it is sometimes easier to glue than to rivet. Many parts, such as wing flaps and floor sections, show greater strength and rigidity for the same weight when joined with tenacious new plastic adhesives. The bonding of metals is now routine with Reanite, a modified rubber manufactured by the United States Stoneware Company, and Cycleweld, a rubber and plastic compound developed by Chrysler Corporation. Ply-metals containing these adhesives are useful in reducing the transmission of vibration particularly in aircraft. Another important application for aircraft is the bonding of plywood to metal. The postwar possibilities are numerous. Plywood, re-enforced internally with corrugated steel, and thin facings of aluminum or stainless steel on plywood are among the more interesting possible applications.

Crack Detection As early as 1929 Sokolov suggested the use of ultrasonics for the detection of defects in large metal castings. Behr[1] and Shrayber[2] have recently extended this idea. Ultrasonic waves travel in well-defined beams in homogeneous substances, but these waves are reflected or dispersed by any inhomogeneity such as a slag inclusion, blow hole, or crack. The distribution of the transmitted beam is measured directly with a piezoelectric detector or can be inferred from the standing waves formed on the surface of an oil bath in which the specimen is immersed.

[1] Behr, Metallurgia **23**, 7 (1940).
[2] Shrayber, Zavod. Lab., p. 816 (1939).

Radioactive Insulin Insulin is the active principle or hormone secreted by the pancreas which enables the body to utilize carbohydrates. Diabetics suffer from a deficiency of insulin, and it is necessary that this substance be given by hypodermic injection. The frequency at which these injections must be administered depends, among other factors, upon the rate of absorption. A more persistent type of insulin, that either is absorbed more slowly from the site of injection or is stored by the body and utilized as needed, would offer a number of advantages over the present forms. By incorporating radioactive iodine, as p-azoiodobenzene, into insulin, globin insulin, and protamine zinc insulin, the rates of absorption of these hormones can be accurately measured by the gamma-radiation emitted from the site of injection. Recent observations on rabbits indicate a decrease in the rate of absorption of these compounds in this order.[1] Additional studies[2] have been made on 4 patients suffering from insulin resistance, 3 patients who had developed fatty pads at the site of repeated injections of insulin, 3 ordinary diabetic patients, and 5 non-diabetic controls. These observations suggest that a delay in the rate of insulin absorption is a major factor in the condition known as insulin resistance.

[1] Reiner, Lang, Irvine, Peacock, and Evans, J. Pharmacol. and Exper. Therapeut. **78**, 352–357 (1943).
[2] Root, Irvine, Evans, Reiner, and Carpenter, J. Am. Med. Assn. **124**, 84–90 (1944).

Gyro Motors Gyroscopes are of major military importance. They hold guns steady; they are an integral part of our bombsights; they direct torpedoes; they help scan the sky for the enemy; they serve in compasses and in numerous other devices. Many special electric motors have been developed to drive gyros at the necessary high angular velocities of several thousand r.p.m. In one instance a gyro flywheel must be brought from rest up to 12,000 r.p.m. in two-tenths of a second. For this purpose Westinghouse builds a motor that weighs but 10.5 pounds, yet develops 22 hp. To provide the armature current of 600 amperes, the brushes must carry a current density of 1600 amperes per square inch.

Bantam gyro motors include several that consume three watts. The rotors for these baby motors—including commutator and shaft—are only about the diameter and length of a thumb. One d.c. shunt-wound, 24-volt motor drives its gyro wheel at 14,000 r.p.m. Two others are supplied with three-phase current, one at 240 cycles (14,000 r.p.m.) and the other at 400 cycles (12,000 r.p.m.). The 240-cycle motor with a rotor less than one inch in diameter and less than one inch long carries a four-pound flywheel. Still another is a single-phase capacitor-type, 3400 r.p.m., 60-cycle motor having an output of only 0.001 hp. These tiny high speed motors must operate under most diverse conditions. At high altitudes or under arctic conditions, they must be able to start their high inertia loads with the temperature at 40° below zero or in the tropics run continuously when the temperature is 130°F. This involves a severe lubrication problem, especially since space for lubrication is small. The motors are totally enclosed and may be confined in tight housings together with other heat-producing apparatus. Only by the use of special low loss iron for a.c. stators and d.c. armatures is it possible to prevent overheating.

Thermometric Indicators The Central Scientific Company has recently developed products for indicating surface temperatures, based upon a series of substances having specific melting points, which offer convenient and accurate means of controlling many industrial and laboratory procedures. The products are available in pellet, crayon, and lacquer form and cover the range from 125 to 1600°F. Distinguishing colors are used for each step of temperature to facilitate identification. Melting occurs within 1 percent of the indicated value. The products are non-corrosive and easily removed after firing.

Spectral Blackouts Familiar physical principles are finding novel military applications. The well-known absorption of green light by a red filter and of the sodium D lines by didymium glass is being used for blackout systems.

Transparent green plastic sheets are used to cover the windows of training planes during instruction in blind flying. The student pilot wears a pair of red plastic goggles made for this purpose by the Polaroid Corporation. As seen in the spectrophotometric curves (see Fig. 1), the green light is completely absorbed by the red filter. Hence, the windows appear black to the student, who is accordingly prevented from seeing out but is free to observe the instrument panel and other objects inside the plane. The instructor, wearing no goggles, sits beside the student and watches out for neighboring planes and other hazards through the green transparent windows. In the past a black cloth was customarily used for this purpose. The new method greatly reduces the risk of collision.

Sodium vapor lamps installed in street cars and buses provide internal illumination without the escape of this light when the windows are made of didymium glass. This

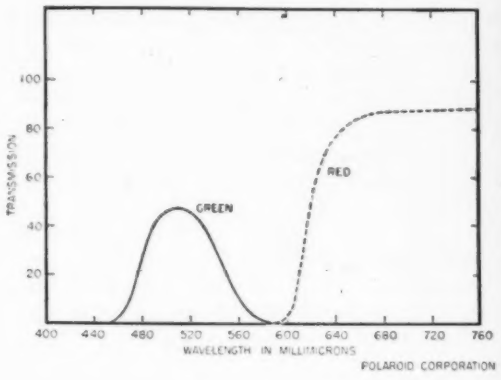

FIG. 1.

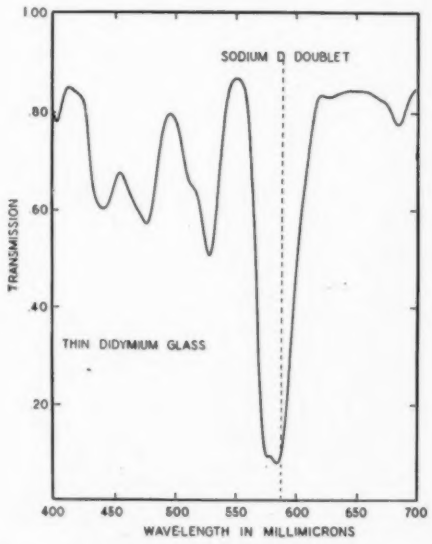

FIG. 2. From the MIT Color Measurement Laboratory.

absorption of the 5893A doubler by didymium is evident from the accompanying curve (Fig. 2). Because of the high transparency to sunlight, the windows appear practically clear during the day.